LA-UR- 09-06018

Approved for public release;
distribution is unlimited.

Title:	EFFECTIVE SHEAR VISCOSITY AND DYNAMICS OF SUSPENSIONS OF MICRO-SWIMMERS AT MODERATE CONCENTRATIONS
Author(s):	V. GYRYA K. LIPNIKOV I. ARONSON L.BERLYAND
Intended for:	JOURNAL: J. MATHEMATICAL BIOLOGY

Los Alamos
NATIONAL LABORATORY
EST. 1943

Form 836 (7/06)

Noname manuscript No.
(will be inserted by the editor)

Effective shear viscosity and dynamics of suspensions of micro-swimmers at moderate concentrations

V. Gyrya · K. Lipnikov · I. Aronson · L. Berlyand

Received: date / Accepted: date

Abstract Recently, there have been a number of experimental studies suggesting that a suspension of self-propelled bacteria (microswimmers in general) may have an effective viscosity significantly smaller than the viscosity of the ambient fluid. This is in sharp contrast with suspensions of hard passive inclusions, whose presence always increases the viscosity. Here we present a 2D model for a suspension of microswimmers in a fluid and analyze it analytically in the dilute regime (no swimmer-swimmer interactions) and numerically using a Mimetic Finite Difference discretization. Our analysis shows that in the dilute regime the effective shear viscosity is not affected by self-propulsion. But at the moderate concentrations (due to swimmer-swimmer interactions) the effective viscosity decreases linearly as a function of the propulsion strength of the swimmers. These findings prove that *(i)* a physically observable decrease of viscosity for a suspension of self-propelled bacteria can be explained purely by hydrodynamic interactions and *(ii)* self-propulsion and interaction of swimmers are both essential to the reduction of the effective shear viscosity.

We performed a number of numerical experiments analyzing the dynamics of swimmers resulting from pairwise interactions. The numerical results agree with the physically observed phenomena (e.g., attraction of swimmer to swimmer and swimmer to the wall). This is viewed as an additional validation of the model and the numerical scheme.

V. Gyrya
The Pennsylvania State University, Department of Mathematics, University Park, PA, 16802, USA
E-mail: gyrya@math.psu.edu

K. Lipnikov
Los Alamos National Laboratory, MS B284, Los Alamos, NM 87545, USA

I. Aronson
Argonne National Laboratory, Division of Material Science, Argonne, IL, USA

L. Berlyand
The Pennsylvania State University, Department of Mathematics, University Park, PA, 16802, USA

1 Introduction

In recent years there have been a number of experimental studies suggesting that self-propulsion can significantly change the rheological properties of suspensions.

In [32] it was shown that self-propelled bacteria (*Escherichia coli*; 1μm wide and 2-3μm long; concentration of swimmers around 10% by volume) by a factor of 2–3 enhanced the diffusion of tracer particles (1-10μm in size) in the quasi-two-dimensional setting of a freely suspended soap film.

More recently, in [29] it was demonstrated that self-propelled bacteria (*Bacillus subtilis*; .7μm wide and 5μm long; concentration of swimmers around 10% by volume) could reduce the viscosity of the suspension (depending on how actively they are swimming) by up to five times when compared to passive/dormant bacteria. Here the experiments were, also, performed in a thin film. The activity of the bacteria was controlled by changing the supply of oxygen. Since bacteria rely on oxygen to convert the chemical energy obtained from the dissolved nutrients into the kinetic energy of swimming, this is an efficient way of controlling the activity of bacteria.

The above experiments demonstrate that suspensions of active inclusions (swimmers) may have drastically different properties than suspensions of passive inclusions. Exploiting these properties may lead to new or improved engineering solutions (e.g., self-replicating micromixers). Explaining and quantifying the changing viscosity for a suspension of swimmers is the goal of this paper.

The effect of self-propulsion on the effective viscosity of the fluid is the major focus of this paper. We identify the following key features affecting the viscosity of a suspension of swimmers and the difficulties related to their modeling and analysis: *(i)* inhomogeneity of the fluid due to inclusions, *(ii)* elongated shape of the inclusions, *(iii)* particle-particle interactions, and the new feature – *(iv)* self-propulsion.

The rheological properties of passive suspensions (suspensions of passive particles) have been studied extensively for over a century. The analysis of the effective viscosity for passive suspensions dates back to the famous work of Einstein [12], where he computed the linear (in volume fraction ϕ) correction to the viscosity for a suspension of neutrally buoyant inert hard spheres in a Newtonian fluid in the dilute limit ($\phi \to 0$).

Jeffery [19] extended the analysis from spherical to ellipsoidal neutrally buoyant inert hard inclusions, where he demonstrated the dependence of the viscosity on the distribution of orientations of the inclusions. Hinch and Leal [21,22] analyzed the limiting distribution of orientations of ellipsoids in a shear flow in the presence of a rotational Brownian motion and used this to obtain the effective viscosity for a suspension of ellipsoids.

Batchelor and Green [2] were the first to consider pairwise particle interactions in order to find the $O(\phi^2)$ correction to Einsteins result [12]. Up to this point, all works have involved formal asymptotics.

In the 1980s, rigorous homogenization results were first obtained for moderate concentrations of particles by Levy and Sanchez-Palencia in [23] and Nunan and Keller in [26] for periodic distributions of inclusions. Results for the densely-packed regime were more recently proven in [7,6,5].

One of the earlier works in modeling the swimming at low Reynolds number was done by Purcell [27]. The modeling of swimmers can be divided into two categories based on whether the model swimmers change their shape or not. Examples of models of swimmers changing their shape are a three-linked sphere swimmer [24,14] and a swimmers with a rotating tail [25]. These models are attractive because the real-world

swimmers (bacteria, fish, etc.) swim due to shape changes (rotation of flagella, waving of the tail, etc.). Unfortunately, the analysis of these models is difficult and at the moment we are not aware of a rheological analysis being done for suspensions of such swimmers, although the dynamics of such swimmer due to their interaction was analyzed in a number of papers (e.g., [25]).

The other category of models are those where the swimmers do not change shape. The propulsion here is either due to a prescribed effective force or an effective relative velocity of the fluid on a part of the surface of the swimmer. Self-propulsion is enforced by equating to zero the total force and torque on each of the swimmers.

Ishikawa and Pedley [18], modeling bacteria as spheres (no elongated body) with a prescribed relative velocity (leads to self-propulsion) on the surface of the spheres, observed a decrease in viscosity only in the presence of a gravitational field. In [18] the results are obtained simulating the dynamics of swimmers using boundary integral methods.

Shelley and Saintillan [28] modeled swimmers as slender rods with tangential tractions prescribed on part of the boundary, for which they observed (in the numerical simulations) behavior reminiscent of that observed in the physical experiment for *Bacillus subtillis* [30]. In particular they observed local nematic ordering of rod-like swimmers that had a significant impact on the mean swimming speed of the swimmers.

In [9] authors consider a phenomenological model of active gels, treating them from the perspective of liquid cristals. In particular they are interested in the effective viscosity of active gels near "nematic" phase. They view suspension of bacteria as one of examples of active gels. In our view attainability of "nematic" phase, understood as an almost perfect ordering in suspesions of swimming bacteria is debatable. On the other hand "nematic" phase may be feasible for suspensions of engineered microswimmers that swim due to externally applied alternating magnetic field (e.g. [10]) and, therefore, could be synchronized to swim in the same direction.

In the recent work [16] Haines, Aranson, Berlyand and Karpeev observed a decrease of the effective viscosity in the dilute limit for slightly elongated spheroids with self-propulsion resulting from a point force in the fluid (attached to the body). They considered two types of background flow: extensional and oscillatory shear flows. In both cases the decrease of viscosity was attributed to swimmers aligning with the flow, supporting the background flow.

In this paper we present a 2D mathematical model of the swimmer-fluid system. The elongated body of the swimmer is modeled by an ellipse. The "front" half of the ellipse represents the solid surface and the "back" half represents the surface covered with flagella that exert the propulsion force onto the fluid.

We consider two concentration regimes: dilute and moderate concentration. In the dilute regime (no swimmer-swimmer interactions) we demonstrate that self-propulsion has no effect on the effective viscosity. Therefore, we show that the elongated shape of the swimmers and the propulsion force are not sufficient to change the effective viscosity as compared to the passive suspensions.

On the other hand decrease of the effective viscosity is observed numerically if all of the above features *(i-iii)* are present: the elongated shape of the swimmers, the propulsion force and the swimmer-swimmer interactions.

To further reflect the settings of the physical experiments in [29] and [32], we studied the suspension at moderate concentrations (approximately 10% by volume). At such concentrations the numerical analysis appears to be the only available tool. The major difficulty in the analysis is the dependence of the apparent viscosity on

the distribution of the swimmers in the fluid domain. The distribution changes with time due to interaction of the swimmers with the ambient flow and other swimmers. Hence, we use the Monte-Carlo approach for measuring the effective viscosity. That is, we solve for the dynamics of the swimmers in the shearing flow, measure the apparent instantaneous viscosity at each time step and average over all time steps.

First, to verify the predictive power of the model and the accuracy of the method we performed a number of tests for the dynamics of swimmers in the proximity of a wall or another swimmer.

Here we observed the attraction of a swimmer to another swimmer and a swimmer to the wall. Heuristically, each swimmer acts as a force-dipole, forcing the fluid away ahead and behind itself and "sucking" the fluid on the sides (due to incompressibility of the fluid). Therefore, the presence of an obstacle to the side of a swimmer forces the swimmer and the obstacle closer to one another due to this "suction".

The attraction in both cases is only short term. A swimmer next to a wall, while getting closer to the wall due to suction, will slowly rotate and swim away form the wall. Two nearby swimmers will swim away from one another once they become offset from the mirror image configuration (see figure 6).

The results, obtained numerically, agreed with the physical observations for *Bacillus subtillis* [30]. At the same time, the results shed light on the details of the swimmer-swimmer and swimmer-wall interactions.

Next we performed a numerical experiment where we measured the effective shear viscosity of a suspension of swimmers in a layer between two solid walls undergoing a shearing motion with relative velocity $2v$. We analyzed the dependence of the measurements of the effective viscosity on the magnitude v of the shearing motion and the propulsion strength of the swimmers, f_p. Using an analytical scaling argument we demonstrated that the effective viscosity depends only on the ratio of the propulsion strength to the magnitude of the shearing motion for a fixed shape of the domain and the swimmers. We call the above ratio the *propulsion-shear ratio*.

Our numerical simulations performed at the moderate concentrations ($\sim$ 10% by volume) indicate that the effective shear viscosity decays linearly as a function of the propulsion-shear ratio of f_p/v. This continues to hold for negative values of the propulsion strength, which corresponds to swimmers swimming in the opposite direction, i.e. pullers instead of pushers. For larger values of the propulsion-shear ratio a deviation from the linear trend was observed and explained.

In section 2 we present a mathematical model for a swimmer in a fluid. Here we write down a complete PDE formulation and motivate each of the choices. In section 2.3 we demonstrate a scaling invariance of the solutions of the PDE, which proves the dependence of the effective shear viscosity on the propulsion-shear ratio. In section 3.1 we introduce the definitions for instantaneous apparent viscosity and the effective shear viscosity, which are the same for homogeneous fluids and generally different for inhomogeneous ones. In section 4 we briefly describe the numerical method, technical difficulties and their solutions followed by the computational results for dynamics of interacting swimmers and the effective shear viscosity for a suspension of swimmers. Finally, in section 5 we summarize the results of our analysis. In appendixes A and B we present the variational formulation for the model and demonstrate the well-posedness of this problem.

2 Mathematical model of a swimmer

In this section we first present the PDE model for a microswimmer in a Stokesian fluid and then motivate every part of the model in section 2.2. The model is written in two dimensions but it can be readily extended to three dimensions.

2.1 The PDE model for the swimmer

Let $\Omega \subset \mathbb{R}^2$ be a bounded domain with a smooth boundary representing the container of the fluid with swimmers. Each swimmer is modeled as an ellipse S^i, $i = 1, \dots, N$ with the center at $\mathbf{x}_C^i$ and the orientation $\mathbf{d}^i$, see Figure 1. Here and below the superscript i indicates the index of the swimmer.

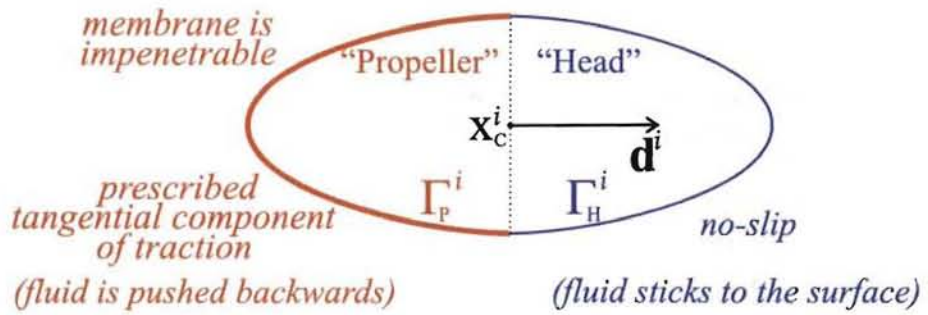

Fig. 1 Illustration of an i-th swimmer with two parts of the boundary: Γ_H^i and Γ_P^i. On the front part Γ_H^i of the swimmer (H stands for "head") the fluid sticks to the surface. On the back part of the swimmer Γ_P^i (P stands for "propeller") the fluid cannot penetrate the boundary of the swimmer. Also, on Γ_P^i the fluid is pushed backwards due to a prescribed tangential component of traction.

The motion of the fluid surrounding the swimmers is governed by the incompressible stationary Stokes equation

$$\begin{cases} \mu \triangle \mathbf{u} = \nabla p \\ \operatorname{div}(\mathbf{u}) = 0 \end{cases} \qquad \text{in } \ \Omega_F := \Omega \setminus \bigcup_i S^i. \tag{1}$$

On the boundary of the fluid domain Ω_F (includes boundaries of the swimmers and the boundary of the container) the following boundary conditions are imposed (in part illustrated in Figure 1):

$$\mathbf{u}(\mathbf{x}) = \mathbf{g}(\mathbf{x}), \qquad \text{for } \mathbf{x} \in \partial\Omega, \tag{2}$$

$$\mathbf{u}(\mathbf{x}) = \mathbf{u}_C^i + \omega^i \times (\mathbf{x} - \mathbf{x}_C^i), \qquad \text{for } \mathbf{x} \in \Gamma_H^i, \tag{3}$$

$$\begin{cases} \left(\mathbf{u}(\mathbf{x}) - [\mathbf{u}_C^i + \omega^i \times (\mathbf{x} - \mathbf{x}_C^i)]\right) \cdot \mathbf{n} = 0 \\ \tau\sigma(\mathbf{u}, p)\mathbf{n} = -f\big((\mathbf{x} - \mathbf{x}_C^i) \cdot \mathbf{d}^i\big)\ (\tau \cdot \mathbf{d}) \end{cases} \qquad \text{for } \mathbf{x} \in \Gamma_P^i, \tag{4}$$

$$\mathbf{F}_H^i + \mathbf{F}_P^i = 0, \qquad \textit{balance of forces}, \tag{5}$$

$$\mathbf{T}_H^i + \mathbf{T}_P^i = 0, \qquad \textit{balance of torques}. \tag{6}$$

Here $\mathbf{u}_C^i$ and ω^i are **unknown** (that need to be found) instantaneous translational and rotational velocities of the i-th swimmer; $\mathbf{n}$ and τ are the unit normal and unit tangent to the surface at the point. The stress tensor $\sigma(\mathbf{u},p)$ is defined by

$$\sigma(\mathbf{u},p) := \mu D(\mathbf{u}) - pI, \qquad D(\mathbf{u}) := \frac{1}{2}\left(\nabla\mathbf{u} + (\nabla\mathbf{u})^T\right); \tag{7}$$

$f(\cdot)$ and $\mathbf{g}(\cdot)$ are the known scalar and vector functions defining the tangential component $\tau\sigma(\mathbf{u},p)\mathbf{n}$ of the traction on Γ_P (see e.g., (14)) and the velocity of the boundary $\partial\Omega$, respectively. The viscous forces $\mathbf{F}_H^i$,$\mathbf{F}_P^i$ and the viscous torques $\mathbf{T}_H^i$,$\mathbf{T}_P^i$ on Γ_H and Γ_P are defined by

$$\mathbf{F}_H^i := \int_{\Gamma_H^i} \sigma(\mathbf{u},p)\mathbf{n}\, d\mathbf{x}, \qquad \mathbf{F}_P^i := \int_{\Gamma_P^i} \sigma(\mathbf{u},p)\mathbf{n}\, d\mathbf{x} \tag{8}$$

and

$$\mathbf{T}_H^i := \int_{\Gamma_H^i} (\mathbf{x}-\mathbf{x}_C^i)\times\sigma(\mathbf{u},p)\mathbf{n}\, d\mathbf{x}, \qquad \mathbf{T}_P^i := \int_{\Gamma_P^i} (\mathbf{x}-\mathbf{x}_C^i)\times\sigma(\mathbf{u},p)\mathbf{n}\, d\mathbf{x}. \tag{9}$$

The PDE problem (1-6) defines the so-called *instantaneous problem*. That is, at any time t the PDE problem (1-6) defines the relation between the positions $\mathbf{x}_C^i(t)$ and orientations $\mathbf{d}^i(t)$ of the swimmers and their translational $\mathbf{u}_C^i(t)$ and rotational $\omega^i(t)$ velocities

$$\mathbf{u}_C^i(t) = \mathbf{U}_C^i\left(\mathbf{x}_C^1(t),\ldots,\mathbf{x}_C^1(t);\mathbf{d}^i(t),\ldots,\mathbf{d}^N(t)\right), \tag{10}$$

$$\omega^i(t) = \Omega^i\left(\mathbf{x}_C^1(t),\ldots,\mathbf{x}_C^1(t);\mathbf{d}^i(t),\ldots,\mathbf{d}^N(t)\right). \tag{11}$$

The values of functions $\mathbf{U}_C^i$ and Ω^i are computed by solving the PDE problem (1-6) for the given positions and orientations of the swimmers. The existence and uniqueness of the solution to the problem (1-6) for the given positions and orientations of the swimmers is outlined in Appendix B.

The dynamics of the swimmers, defining the evolution of the fluid domain $\Omega_F(t) = \Omega\setminus\bigcup_i S^i(t)$, is given by the ODE ($i=1,\ldots,N$)

$$\begin{cases} \frac{d}{dt}\mathbf{x}_C^i(t) = \mathbf{u}_C^i(t) & = \mathbf{U}_C^i\left(\mathbf{x}_C^1(t),\ldots,\mathbf{x}_C^1(t);\mathbf{d}^i(t),\ldots,\mathbf{d}^N(t)\right), \\ \frac{d}{dt}\mathbf{d}^i(t) = \mathbf{d}^i(t)\times\omega^i(t) & = \mathbf{d}^i(t)\times\Omega^i\left(\mathbf{x}_C^1(t),\ldots,\mathbf{x}_C^1(t);\mathbf{d}^i(t),\ldots,\mathbf{d}^N(t)\right) \end{cases} \tag{12}$$

with the initial conditions

$$\mathbf{x}_C^i(0) = \mathbf{x}_C^{i,0}, \qquad \mathbf{d}_C^i(0) = \mathbf{d}_C^{i,0}, \quad \left|\mathbf{d}_C^{i,0}\right| = 1. \tag{13}$$

2.2 Discussion and motivation for the PDE model

Here we present the motivation for the above PDE model and discuss some issues related to modeling.

First of all, the modeling of the fluid motion by an incompressible stationary Stokes equation (1) is a fairly standard reduction from the Navier-Stokes PDE for small Reynolds number, $\mathcal{R}e := \frac{\rho V L}{\mu} 1 \ll 1$. Here ρ is the density of the fluid ($\rho \approx 1\mathrm{g/cm}^2$), V and L are representative velocities and sizes in the problem. For instance, on the

scale of self-propelled bacteria, such as *Bacillus Subtilis* (5μm in length and $.7\mu$m in width, swimming with the velocity up to 100μm/sec) $\mathcal{R}e \approx 10^{-4} \ll 1$.

Next we discuss the boundary conditions for the incompressible Stokes equation. The boundary condition (2) indicates that the fluid sticks to the walls of the container Ω, which are moving with velocity $\mathbf{g}(\mathbf{x})$. This is a standard boundary condition for solid walls. It can also be applied to the case of bacteria in a thin film. The boundary $\partial\Omega$ of the container Ω, here, would be the fluid-air interface. The reason for using the no-slip boundary condition would be the fact that bacteria produce a surfactant that solidifies the interface [30].

The boundary condition (3) is similar to the condition (2) in that the fluid sticks to the surface Γ_H^i. But unlike $\partial\Omega$, the boundary Γ_H^i is moving with translational velocity $\mathbf{u}_C^i$ and rotational velocity ω^i that are not known a priori and need to be found in the process of solving (1-6).

The boundary condition $(4a)$ indicates that the fluid cannot flow through the surface Γ_P^i of the swimmer, moving with translational velocity $\mathbf{u}_C^i$ and rotational velocity ω^i. Also, there is a force acting on the fluid on the surface Γ_P^i that pushes the fluid backward, as a result propelling the swimmer forward. Since there is a condition of "no flow through Γ_P^i" $(4a)$, one can only prescribe the tangential component of the traction $\sigma(\mathbf{u},p)\mathbf{n}$ on Γ_P^i. This is done by $(4b)$.

Note that the form of the RHS of $(4b)$ indicates that the propulsion of the swimmer is coordinate invariant, since it is given in terms of the coordinate invariant operators: scalar and vector products. More precisely, the propulsion is invariant under rotation and translation of coordinate system.

An example of the tangential component of traction defined by $(4b)$ is the "uniform" distribution over Γ_P

$$\tau\sigma(\mathbf{u},p)\mathbf{n} = -f\big((\mathbf{x}-\mathbf{x}_C^i)\cdot\mathbf{d}^i\big)\ (\tau\cdot\mathbf{d}^i) := \frac{-f_p}{|\Gamma_P|}\ (\tau\cdot\mathbf{d}^i), \tag{14}$$

where f_p is the "total force of the propulsion" (directed backward):

$$f_p = \int_{\Gamma_P} f\big((\mathbf{x}-\mathbf{x}_C^i)\cdot\mathbf{d}^i\big)\ dx. \tag{15}$$

Boundary conditions (5) and (6) indicate that all swimmers are self-propelled as opposed to moving due to an external force (e.g., gravity). One can obtain equations (5)-(6) from Newton's second law, noting that in the Stokes regime the inertial forces are negligible compared to the viscous forces (for more details see [15]).

2.3 Scaling observation

The following observation will be important to simplify the future analysis. Consider two initial value problems (1-12), with the same initial data (i.e., positions of the swimmers $\left\{\mathbf{x}_C^i(0),\mathbf{d}^i(0)\right\}$ and the same domain Ω) but different boundary conditions, related by a scaling:

Problem I: The boundary data

$$\mathbf{g}^I(t,\mathbf{x}) \qquad \text{and} \qquad f^I(s). \tag{16}$$

Problem II: The boundary data

$$\mathbf{g}^{II}(t,\mathbf{x}) = \lambda \mathbf{g}^{I}(t/\lambda,\mathbf{x}) \qquad \text{and} \qquad f^{II}(s) = \lambda f^{I}(s). \tag{17}$$

Denote the solutions of problem I above (i.e., the motion of swimmers and the velocity of the fluid at time t and point $\mathbf{x}$) by

$$\mathbf{x}_C^{i,I}(t), \mathbf{d}^{i,I}(t) \text{ with } i = 1,\dots,N \qquad \text{and} \qquad \mathbf{u}^{I}(t,\mathbf{x}). \tag{18}$$

Then the following scaling holds for the solution of problem II.

Lemma 1 (Scaling) *Function*

$$\mathbf{u}^{II}(t,\mathbf{x}) := \lambda \mathbf{u}^{I}(t/\lambda,\mathbf{x}) \tag{19}$$

and the motion of the swimmers

$$\mathbf{x}_C^{i,II}(t) = \mathbf{x}_C^{i,I}\left(\frac{t}{\lambda}\right), \qquad \mathbf{d}^{i,II}(t) = \mathbf{d}^{i,I}\left(\frac{t}{\lambda}\right) \tag{20}$$

solve problem II.

Proof Let's check that $\mathbf{u}^{II}(t,\mathbf{x})$, as defined by (19), is, indeed, a solution of the time-dependent problem II.

It is easy to check that $\mathbf{u}^{II}(t,\mathbf{x})$ is a solution of the instantaneous problem (1-6) with boundary data given by (16) and the velocities of the swimmers

$$\mathbf{u}_C^{i,II}(t) = \lambda \mathbf{u}_C^{i,I}\left(\frac{t}{\lambda}\right), \qquad \omega^{i,II}(t) = \lambda \omega^{i,I}\left(\frac{t}{\lambda}\right). \tag{21}$$

Since (18) is a solution of problem I the motion of the swimmers (20) satisfies the following ODE

$$\begin{cases} \frac{d}{dt}\mathbf{x}_C^{i,II}(t) = \lambda \frac{d}{dt}\mathbf{x}_C^{i,I}\left(\frac{t}{\lambda}\right) = \lambda \mathbf{u}_C^{i,I}\left(\frac{t}{\lambda}\right) = \mathbf{u}_C^{i,II}(t), \\ \frac{d}{dt}\mathbf{d}^{i,II}(t) = \lambda \mathbf{d}^{i,I}\left(\frac{t}{\lambda}\right) = \lambda \mathbf{d}^{i,I}\left(\frac{t}{\lambda}\right) \times \omega^{i,I}\left(\frac{t}{\lambda}\right) = \mathbf{d}^{i,II}\left(\frac{t}{\lambda}\right) \times \omega^{i,II}(t). \end{cases} \tag{22}$$

This is exactly the ODE (12) for the motion of the swimmers in the problem II.

We summarize the above observation as follows:

Remark 1 *Simultaneously increasing the propulsion force $f(\cdot)$ of the swimmers and the velocity of the fluid $\mathbf{g}(\mathbf{x})$ on the boundary $\partial\Omega$ by a factor of λ leads to swimmers moving on the same trajectories but λ times faster. The corresponding viscous forces, also, increase by a factor λ.*

3 Effective viscosity

In the theory of fluid dynamics one of the primary objects of interest is the relation between the applied forces (stress) and the observed fluid flow (strain rate). For Newtonian fluids this relationship is linear

$$\sigma_{ij}(\mathbf{x}) = \mu\dot{\varepsilon}_{ij}(\mathbf{x}) \qquad \text{for } \mathbf{x} \in \Omega_F,\ i \neq j, \qquad \dot{\varepsilon}(\mathbf{x}) := \frac{1}{2}\left(\nabla\mathbf{u} + (\nabla\mathbf{u})^T\right) \tag{23}$$

and is defined by a scaling constant μ, called viscosity.

For non-Newtonian fluids (23) does not hold with the same value of μ. Hence, assuming that one still desires to characterize the relation between the stress and the strain rate in the form similar to (23), the viscosity μ should be permitted to vary. What should μ depend on?

In the most general case, μ will depend on the form of the flow (i.e. on the strain rate: $\mu(\varepsilon)$). This is not very informative, as in this case the relation $\sigma = \mu(\dot{\varepsilon})\dot{\varepsilon}$ is equivalent to $\sigma = f(\dot{\varepsilon})$, where $f(\cdot)$ is some function. So, to answer the question about the relation between the stress and the strain rate, one should specify the function $f(\cdot)$.

To avoid this problem, accept the fact that the general relation between the bulk stress and the bulk strain rate greatly depends on the type of the fluid flow. Thus we will limit ourselves to a rather specific, but very experimentally intuitive definition along the lines, proposed by G.K. Batchelor [1]:

> We shall consider here only the important and representative case in which the suspension is confined between two parallel rigid planes in steady relative shearing motion, with the stress being observed as the force per unit area on a section of one boundary with linear dimensions large compared with particle spacing.
>
> Our definition of the effective shear viscosity will be similar to the above one.

3.1 Definition of effective viscosity and instantaneous apparent viscosity

Consider a fluid (or a complex fluid, such as a suspension of active or passive particles in the fluid) between two solid plates a distance $2H$ apart, see Figure 2. We induce a shearing motion on the boundary by moving the top plate (right) with velocity $v\mathbf{e}_1$ and the bottom plate (left) with velocity $-v\mathbf{e}_1$. For completeness of the definition of the motion on the boundary we prescribe the periodic conditions on the left and right boundary. The effective shear viscosity $\hat{\mu}(v)$, being a measure of friction in the fluid, then should be defined in terms of the total viscous forces $\mathbf{F}_T$ and $\mathbf{F}_B$, acting on the top and the bottom plates, respectively. In case of suspensions, the viscous forces may depend on the distribution of inclusions and, hence, be functions of time. Also, the effective shear viscosity should scale correctly with the dimensions of the domain

$$\bar{\mu}(v;t) := \frac{H}{Lv}\left(\mathbf{F}_T(t) - \mathbf{F}_B(t)\right)\cdot\mathbf{e}_1, \tag{24}$$

where L is the length of the plate.

The definition (24) makes a perfect sense for homogeneous fluids, where viscous forces $\mathbf{F}_T$ and $\mathbf{F}_B$ do not change with time. For non-homogeneous fluid there are additional challenges. For instance, for a suspension of passive or active inclusions the

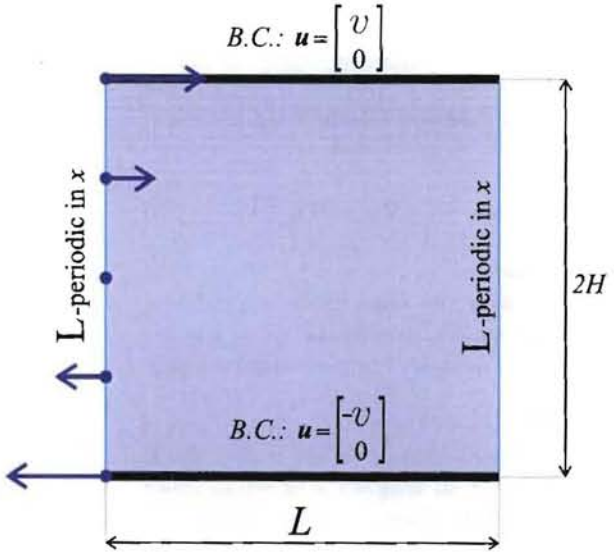

Fig. 2 Schematic illustration of shear flow between two plates.

value of $\hat{\mu}(v)$ in (24) will be different depending on the concentration and distribution of inclusions. For a suspension of active inclusions, such as swimmers, it will also depend on the propulsion strength of the swimmers. Moreover, changing the propulsion strength from f_p to $-f_p$, in general, will change $\hat{\mu}(v)$ in (24) in a nontrivial way: *(i)* it will not remain the same and *(ii)* it will not just change sign. For this reason, we do not call the quantity in (24) – effective viscosity. Instead, (24) is called *instantaneous apparent viscosity*. Here, *instantaneous* indicates that the quantity (24) is computed instantly and depends on a particular configuration. The word *apparent* indicates the nontrivial dependence on the propulsion strength. This dependence will be analyzed later in section 3.2.1.

We wish to define the effective viscosity as a material property independent of the configuration of swimmers. Thus, we define the *effective viscosity* as a time average of the instantaneous apparent viscosity

$$\hat{\mu}(v) := \int_0^\infty \bar{\mu}(v;t)\, dt. \tag{25}$$

We assume that this time-averaged quantity does not depend on the initial configuration of swimmers.

3.2 Estimates and observations for the apparent viscosity

Here we make some analytic observations regarding the instantaneous apparent measurements of effective viscosity. First, we make use of the scaling observation, Remark 1. This observation tells us that the apparent viscosity, as defined by (24), takes the

same value for problems I and II, (16-17), at times t/λ and t:

$$\begin{aligned}\hat{\mu}^{II}(\lambda v, \lambda f_p; t/\lambda) &= \frac{H}{L\lambda v}\left(\mathbf{F}_T^{II}\left(\frac{t}{\lambda}\right) - \mathbf{F}_B^{II}\left(\frac{t}{\lambda}\right)\right)\cdot \mathbf{e}_1 = \\ &= \frac{H}{Lv}\left(\mathbf{F}_T^{I}(t) - \mathbf{F}_B^{I}(t)\right)\cdot \mathbf{e}_1 = \hat{\mu}^{I}(v, f_p; t)\end{aligned} \tag{26}$$

Hence the effective viscosities, being time averages of the instantaneous apparent viscosities, also, match for the problems I and II:

$$\begin{aligned}\hat{\mu}^{II}(\lambda v, \lambda f_p) &= \lim_{T\to\infty}\frac{1}{T}\int_0^T \hat{\mu}^{II}(\lambda v, \lambda f_p; t/\lambda)\, dt = \\ &= \lim_{T\to\infty}\frac{1}{T}\int_0^T \hat{\mu}^{I}(v, f_p; t)\, dt = \hat{\mu}^{I}(v, f_p).\end{aligned} \tag{27}$$

This means that the effective viscosity of a suspension of swimmers depends only on the ratio of propulsion strength of the swimmers f_p to the shear rate defined by v, i.e.

$$\hat{\mu}\left(\frac{v}{f_p}\right) := \hat{\mu}\left(\frac{v}{f_p}, 1\right) = \hat{\mu}\left(1, \frac{f_p}{v}\right). \tag{28}$$

Due to its importance we call the ratio f_p/v – the *propulsion-shear ratio.*

3.2.1 The apparent viscosity for the instantaneous problem

In this section we consider the instantaneous problem (1-6) in the fluid domain $\Omega_F = \Omega \setminus \cup_i S_i$. We want to identify the dependence of the instantaneous apparent viscosity on the propulsion strength f_p of the swimmers for a given distribution of swimmers.

We will consider three instantaneous problems **A-C** given by (1-6) with the same fluid domain Ω_F, but different boundary conditions:

A. Active swimmers + Shear: The shear velocity $v^{\mathrm{A}} = v$ and the propulsion strength of the swimmers $f_p^{\mathrm{A}} = f_p$ are non-zero.

B. Passive/dormant swimmers + Shear: The shear velocity $v^{\mathrm{B}} = v^{\mathrm{A}}$ is non-zero, but the propulsion strength of the swimmers f_p^{B} is zero.

C. Active swimmers + No shear: The shear velocity $v^{\mathrm{C}} = 0$ is zero, but the propulsion strength of the swimmers $f_p^{\mathrm{C}} = f_p^{\mathrm{A}}$ is nonzero.

Due to the linearity of the Stokes equation (1) the solution $(\mathbf{u}^{\mathrm{A}}, p^{\mathrm{A}})$ of the problem **A** is a sum of the solutions $(\mathbf{u}^{\mathrm{B}}, p^{\mathrm{B}})$ and $(\mathbf{u}^{\mathrm{C}}, p^{\mathrm{C}})$ to the problems **B** and **C**:

$$\mathbf{u}^{\mathrm{A}}(\mathbf{x}) = \mathbf{u}^{\mathrm{B}}(\mathbf{x}) + \mathbf{u}^{\mathrm{C}}(\mathbf{x}) \qquad \text{and} \qquad p^{\mathrm{A}}(\mathbf{x}) = p^{\mathrm{B}}(\mathbf{x}) + p^{\mathrm{C}}(\mathbf{x}). \tag{29}$$

We have a similar relation for the forces on the top and bottom plates, the expression that enters the definition (24) of the instantaneous apparent viscosity:

$$\left(\mathbf{F}_T^{\mathrm{A}}(v, f_p) - \mathbf{F}_B^{\mathrm{A}}(v, f_p)\right) = \left(\mathbf{F}_T^{\mathrm{B}}(v) - \mathbf{F}_B^{\mathrm{B}}(v)\right) + \left(\mathbf{F}_T^{\mathrm{C}}(f_p) - \mathbf{F}_B^{\mathrm{C}}(f_p)\right). \tag{30}$$

Here we explicitly indicated that the forces depend on the shear velocity v and the propulsion strength of the swimmers.

Using the definition (24), we get

$$\begin{aligned}\bar{\mu}^{\mathrm{A}}(v, f_p) &= \frac{H}{Lv}\left(\mathbf{F}_T^{\mathrm{A}}(v, f_p) - \mathbf{F}_B^{\mathrm{A}}(v, f_p)\right)\cdot \mathbf{e}_1 = \\ &= \frac{H}{Lv}\left(\mathbf{F}_T^{\mathrm{B}}(v) - \mathbf{F}_B^{\mathrm{B}}(v)\right)\cdot \mathbf{e}_1 + \frac{H}{Lv}\left(\mathbf{F}_T^{\mathrm{C}}(f_p) - \mathbf{F}_B^{\mathrm{C}}(f_p)\right)\cdot \mathbf{e}_1 = \\ &= \hat{\mu}^{\mathrm{B}}(v) + \frac{H}{Lv}\bar{\eta}(f_p),\end{aligned} \tag{31}$$

where

$$\frac{H}{Lv}\bar{\eta}(f_p) := \frac{H}{Lv}\left(\mathbf{F}_T^{\mathrm{C}}(f_p) - \mathbf{F}_B^{\mathrm{C}}(f_p)\right)\cdot \mathbf{e}_1 \tag{32}$$

is the contribution to the instantaneous apparent viscosity due to self-propulsion.

Note that if $\left(\mathbf{F}_T^{\mathrm{C}}(f_p) - \mathbf{F}_B^{\mathrm{C}}(f_p)\right)\cdot \mathbf{e}_1 \neq 0$, the RHS blows up in the limit of small shear rates (constant $f_p \neq 0$), i.e.

$$\lim_{v\to 0} \hat{\mu}^{\mathrm{A}}(v) = \infty. \tag{33}$$

On the other hand for large shear rates (constant f_p) the apparent viscosity $\hat{\mu}^{\mathrm{A}}$ approaches the apparent viscosity $\hat{\mu}^{\mathrm{B}}$ of passive/dormant swimmers

$$\lim_{v\to \infty} \hat{\mu}^{\mathrm{A}}(v) = \hat{\mu}^{\mathrm{B}}(v). \tag{34}$$

3.3 Effective shear viscosity for a suspension of swimmers in the dilute regime

Consider a suspension of swimmers in the dilute regime: the fluid domain is sufficiently large and swimmers are sufficiently far apart from one another. Thus, the dilute assumptions consist of the following: *(i)* individual swimmers interact only with the background flow and do not interact with one another, *(ii)* positions of the swimmers are not important, only their orientations play any role in the effective viscosity.

A consequence of *(i)*, *(ii)* and the decomposition of the instantaneous problem (1-6) in section 3.2.1 are the following.

Lemma 1 *The rotational velocity of swimmers is an even function of θ, i.e.*

$$\omega(\theta) = \omega(-\theta). \tag{35}$$

Proof Indeed, the rotation of swimmers is entirely due to the background flow and does not depend on the propulsion strength f_p of the swimmers. That is the rotational velocity $\omega = \omega(\theta)$ is a function of the orientation of the swimmer. Due to the symmetry of the flow we get (35).

Let $p(\theta)$ be the density function for the portion of time that a swimmer spends at the angle θ,

$$\int_{-\pi}^{\pi} p(\theta)\, d\theta = 1.$$

Lemma 2 *The density function $p(\theta)$ is an even function of θ, i.e.*

$$p(\theta) = p(-\theta). \tag{36}$$

Proof The statement (36) follows from Lemma 1 and the conservation of flux condition

$$p(\theta)\omega(\theta) = \text{constant for all } \theta.$$

Now consider the contribution to the instantaneous apparent viscosity $\eta(f_p;t)$ due to self-propulsion as introduced in (31) and (32).

Lemma 3 *The total contribution $\hat{\eta}(f_p)$ to the effective viscosity due to self propulsion, defined as the time average of the contribution $\bar{\eta}(f_p;t)$ to the instantaneous apparent viscosity due to self-propulsion is zero:*

$$\hat{\eta}(f_p) := \int_0^\infty \bar{\eta}(f_p;t)\ dt = \int_0^\infty \left(\mathbf{F}_T^C(f_p;t) - \mathbf{F}_B^C(f_p;t)\right)\cdot \mathbf{e}_1\ dt = 0. \tag{37}$$

Proof The contribution of the swimmers $\bar{\eta}(f_p;t)$ due to self-propulsion is a sum of contributions due to each each swimmer

$$\bar{\eta}(f_p;t) = \sum_{i=1}^{N} \bar{\eta}_i(f_p,\theta),$$

which are completely determined by their orientations (N is total number of swimmers).

Also, from the symmetry of the flow the contribution to the instantaneous apparent viscosity $\bar{\eta}(\theta)$ due to self-propulsion of a swimmer having angle θ is minus that of a swimmer having angle $-\theta$:

$$\bar{\eta}(\theta) = -\bar{\eta}(-\theta)$$

Hence, the total contribution to the instantaneous apparent viscosity due to self-propulsion of all swimmers is

$$\begin{aligned}\int_{-\pi}^{\pi} p(\theta)\bar{\eta}(\theta)\ d\theta &= \int_{-\pi}^{0} p(\theta)\bar{\eta}(\theta)\ d\theta + \int_0^{\pi} p(\theta)\bar{\eta}(\theta)\ d\theta = \\ &= -\int_0^{\pi} p(\theta)\bar{\eta}(\theta)\ d\theta + \int_0^{\pi} p(\theta)\bar{\eta}(\theta)\ d\theta = 0.\end{aligned}$$

From the definition of the effective viscosity (25), decomposition of instantaneous apparent viscosity (31), independence of the dynamics of the orientation of swimmers on the propulsion strength and, finally, Lemma (3) we get the following statement.

Theorem 1 *The effective viscosity of a suspension of swimmers interacting only with the background shear flow is the same as the effective viscosity of a suspension of passive inclusions.*

4 Numerical modeling and analysis

We solve the ODE (12) using forward Euler method with variable time step $\triangle t_n$ (see more on the choice of the time-step in section 4.2). On each time step t_n for known positions $\mathbf{x}_C^i(t_n)$ and orientations $\mathbf{d}^i(t_n)$ we find velocities of the swimmers (that is evaluate the implicit functions $\mathbf{U}_C^i$ and Ω_C^i) by solving the PDE problem (1-6). Using the newly obtained translational and rotational velocities, we update the positions of the swimmers, assuming constant velocities on the time interval $(t_n, t_n + \triangle t_n)$,

$$\mathbf{x}_C^i(t_{n+1}) = \mathbf{x}_C^i(t_n) + \triangle t_n \mathbf{v}_C^i(t_n). \tag{38}$$

4.1 Solution of the instantaneous problem

Solution of the PDE problem (1-6) on each time step is the key for obtaining the dynamics of swimmers and for computing the viscosity of the suspension. To solve the PDE problem (1-6) we use the recently developed Mimetic Finite Difference (MFD) method [3]. Since MFD method for the Stokes problem is a new method, below we give short comparison description between this method and some other popular methods.

4.1.1 Short description of MFD method

The MFD method combines mesh flexibility of the Finite Volume (FV) methods with analytical power of Finite Element (FE) methods. To some extend it can be viewed as an extension of FE methods to unstructured polygonal (polyhedral in three dimensions) meshes. The mesh flexibility simplifies mesh generation around swimmers that may have complicated shapes. The major difference between the MFD and FE methods lies in definition of basis functions. The FE methods define then explicitly everywhere in the computational domain. The MFD method specifies the basis functions only on mesh edges. This reduction of topological complexity has a number of important consequences for numerical modeling of complex phenemona.

First, the MFD method minimizes the number of discrete unknowns (compared to the FE method) (a) by partitioning of the computation domain into smaller number of elements that are polygons and (b) by using velocity and pressure degrees of freedom only where they are needed for accuracy and stability of the discretization. For example, the MFD method on a square mesh with N mesh vertices uses about $2.5N$ velocity and N pressure unknowns. The FE methods on the same mesh and with roughly the same accuracy uses about $4N$ velocity and N pressure unknowns.

Second, the MFD method is build the same way on general polygonal meshes as on triangular meshes. Thus, the MFD method can be used on locally refined meshes with hanging nodes and on moving meshes with non-convex elements that are frequently used in numerical modeling. It was shown in [8] that the MFD method can be employed even when the mesh elements have curved faces. In this work, we use polygonal meshes near boundary of the swimmers (see section 4.1.2) and make the computational mesh coarser far away from the swimmers. This approach increases accuracy in the areas of interest. The MFD method we employ is the second-order accurate (with respect to the local mesh size) for the velocity and the first-order accurate for the pressure.

4.1.2 Mesh construction

In the simulations performed for this paper we used the following mesh construction. Since the intricate part of the mesh construction is around swimmers, we divided the whole process into three parts: constructing the "background" mesh, overlapping the "background" mesh with the swimmers, and coarsening the mesh away from the swimmers and the walls.

First we construct a "background" mesh, which we chose to be uniform square mesh, i.e. the square domain of size 1 by 1 is divided into N^2 squares with sides $h = 1/N$.

We then overlap the "background" mesh with the ellipses representing swimmers. For this we find the points of intersection of the ellipses with the edges of the "background" mesh. These points are connected by straight edges and added to the new

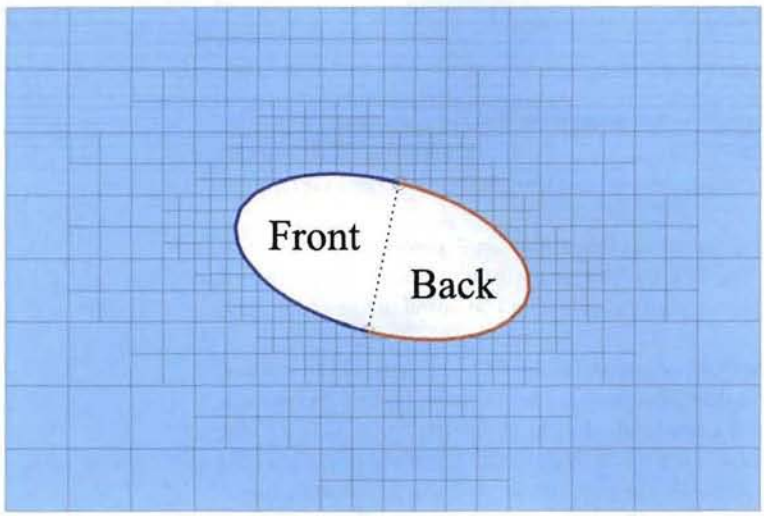

Fig. 3 A sample mesh near a swimmer. The computational domain is around the swimmer and is colored light blue. The mesh is coarsened away from the swimmer. Notice that the mesh elements adjacent to the swimmer are polygons with 3, 4 and 5 vertices.

mesh. The mesh elements inside the ellipses are then thrown out. As a result, the boundary of the ellipses is approximated by polygons based on the points of intersection of the ellipses with the background mesh (see Figure 3).

Since the boundary of the ellipses is approximated using polygons it is important to have a fine mesh around the ellipses. Also, the spacial variations of the flow for the solutions are largest around the boundaries. Hence, to capture these variations mesh size should be smaller next to the boundaries. On the other hand away from the boundaries we may coarsen the mesh without significuntly increasing the numerical error. We coarsen the mesh by grouping the mesh elements with centers at least $2h$ away from the boundary into square mesh elements with sides $2h$. This process can be perfored again, grouping the mesh elements with centers at least $4h$ away from the boundary into square mesh elements with sides $4h$.

4.2 Choosing the time step

There are several factors that determine the size of the time step $\triangle t_n$. For moderate concentrations of swimmers ($\sim 10\%$ by volume) the crucial point here is to avoid collisions of swimmers. For this, the relative displacements of the swimmers on each time step should be small compared to their pairwise distances. Due to the hydrodynamic attraction of swimmers it is common to see pairs of swimmers arbitrarily close to one another. This requires to have "arbitrarily small" time step. This is not practical as there is no lower bound on the time step (i.e., there is no a priori estimate on the amount of computer time to simulate 1 second of "real" time).

We implemented a balanced algorithm for choosing the time step. We decide on the upper $\triangle t_{\text{upper}}$ and the lower $\triangle t_{\text{lower}}$ bounds for the time step (e.g. $\triangle t_{\text{upper}} := .01$, $\triangle t_{\text{lower}} := .001$ for $f_p = 1$). Then at each time step, after computing the translational

and rotational velocities we pick the size of the time step $\triangle t$

$$\triangle t_{\text{upper}} \geq \triangle t \geq \triangle t_{\text{lower}}$$

so as to avoid swimmers getting closer than the mesh size h to one another.

It may not be possible to chose $\triangle t \leq \triangle t_{\text{lower}}$ so as to avoid collisions. If this is the case, we choose the time step $\triangle t := \triangle t_{\text{lower}}$ and adjust the positions of the overlapping swimmers.

Numerical experiments show that choosing the upper and lower bounds for the time steps $\triangle t_{\text{upper}} := .01$, $\triangle t_{\text{lower}} := .001$ for the propulsion strength of swimmers $f_p = 1$ and the shear rate $\dot{\gamma} = 1$ leads to smooth changes in the apparent viscosity (see figure 7).

The choice of the time step for the cases of larger values of the propulsion strength of the swimmers $f_p > 1$ is based on the scaling observation (see Remark 1). Due to Remark 1 the trajectories of swimmers obtained numerically for the case with $\dot{\gamma} = 1, f_p = f_p^0$ and $\triangle t = \triangle t^0$ will be the same as in the case with $\dot{\gamma} = 1/\lambda, f_p = f_p^0/\lambda$ and $\triangle t = \triangle t^0/\lambda$. We choose the scaling constant $\lambda = f_p$, i.e. we fix the propulsion strength of the swimmers. This leads to smaller values of the shear rate than in the base case. Therefore, our choice of the upper and lower bounds for the time step for $\dot{\gamma} = 1$ and $f_p > 1$ is $\triangle t_{\text{upper}} := .01/f_p$, $\triangle t_{\text{lower}} := .001/f_p$.

4.3 Implementing collisions of swimmers

We attempt to avoid the collisions between swimmers through dynamically changing the time step. Still, this only minimizes the chances of collisions and does not completely eliminate the possibility of them happening. Thus, we need to have a numerical block that handles the collisions.

To avoid any additional difficaulties with the accuracy of the method, we consider a small exclusion region around each swimmers (roughly, all points distance h away from the swimmer). The exclusion region for the swimmer represented by an ellipse with major semi-axis a and b is taken to be an ellipse with major semi-axis $a + h$ and $b + h$, respectively. Therefore, if the exlusion regions of two swimmers do not overlap then these swimmers are guaranteed not to have a common mesh element adjacent to both. The collision is implemented as a soft collision of eclusion regions, where the place of mass is taken by the viscous drag coefficients of the ellipses.

Consider two ellipses in contact. The force of their interaction is directed along the normal to their surfaces at the point of the contact. The force $\mathbf{F}_{1,2}$ of the first swimmer S_1 onto the second swimmer S_2 is equal in magnitude and opposite in direction to $\mathbf{F}_{2,1}$, the force of S_2 onto S_1

$$\mathbf{F}_{1,2} = -\mathbf{F}_{2,1}. \tag{39}$$

To observe the effect of the interaction force $\mathbf{F}_{2,1}$ on the motion of the swimmer S_1, we compute the net force and the net torque produced on the swimmer:

$$\mathbf{F}^1_{\text{net}} = \mathbf{F}_{2,1} \qquad \text{and} \qquad T^1_{\text{net}} = \mathbf{F}_{2,1} \times (\mathbf{x} - \mathbf{x}^1_C). \tag{40}$$

The force $\mathbf{F}_{2,1}$ will be acting on swimmer S_1 as long as S_1 and S_2 are in contact. In the Stokes regime (where inertia is negligible compared to the viscous forces) the forces $\mathbf{F}_{2,1}$ and $\mathbf{F}_{1,2}$ will be only as strong as necessary to prevent penetration of swimmer by the other.

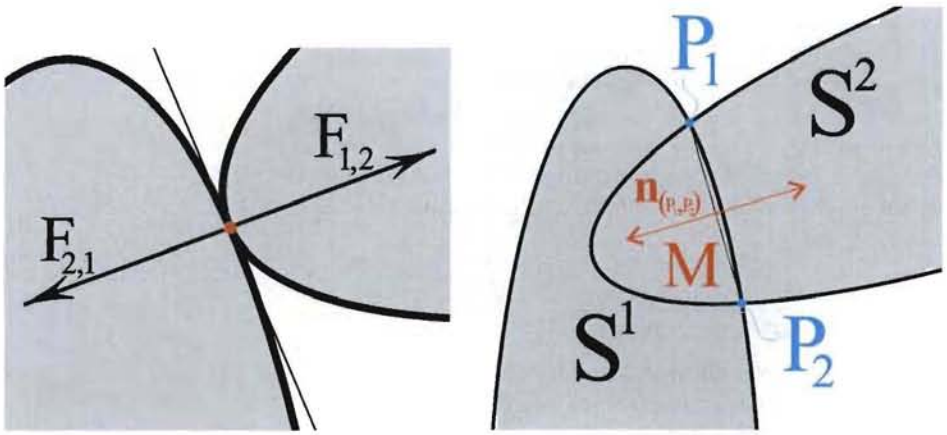

(a) (b)

Fig. 4 Two ellipsoidal swimmers in contact *(a)* and two overlapping ellipsoidal swimmers *(b)*.

Also, in the Stokes regime the role of the mass (since inertia forces are dominated by viscous forces) is played by the viscous drag coefficients. We have three drug coefficients: γ_a,γ_b, and γ_θ, two for translational motions – (γ_a) along major and (γ_b) along minor axis, and γ_θ for the rotational motion.

If τ is the direction of the major axis and $\tau_\perp$ is the direction of the minor axis, write $\mathbf{F} = f_a\tau + f_b\tau_\perp$. We write the motion of the ellipse as $\mathbf{v}_C = f_a\tau + f_b\tau_\perp$ and ω. Then the drag coefficients relate the forces acting on the ellipse with the motion of the ellipse as follows

$$f_a = \gamma_a v_a, \qquad f_b = \gamma_b v_b, \qquad T = \gamma_\theta \omega. \tag{41}$$

Now, suppose at time t_0 we solved the Stokes problem for two swimmers S_1 and S_2 and found their velocities $\mathbf{v}_i$ and ω_i, $i = 1, 2$. We wish to adjust the positions of the swimmers according to this velocities to compute the positions at time $t_1 = t_0 + \triangle t$. We compute these positions and orientations as

$$\mathbf{x}^i_{(1)} = \mathbf{x}^i_{(0)} + \triangle t\, \mathbf{v}^i_{(0)}$$

and similarly for the orientations.

Suppose, the time step $\triangle t \geq \triangle t_{\text{lower}}$ cannot be chosen so as to avoid overlap of the exclusion regions. Then we take $\triangle t = \triangle t_{\text{lower}}$.

For two overlapping ellipses, as on Fig. 4*(b)*, in general there will be two points of intersection P_1, P_2. Find the midpoint $M := (P_1 + P_2)/2$. This midpoint will be considered as the point of the interaction. The interaction force will be assumed to act perpendicular to the line $(P1, P2)$: $\mathbf{n}_{(P1,P2)}$ on S^1 and $-\mathbf{n}_{(P1,P2)}$ on S^2. Based on this information we can compute the correction velocities of the swimmers

$$\begin{aligned} v^1_a &= \gamma_a^{-1} f_a = \gamma_a^{-1} \tau_a \cdot \mathbf{n}_{(P1,P2)}, \\ v^1_b &= \gamma_b^{-1} f_b = \gamma_b^{-1} \tau_b \cdot \mathbf{n}_{(P1,P2)}, \\ \omega^1 &= \gamma_\theta^{-1} T = \gamma_\theta^{-1} \mathbf{n}_{(P1,P2)} \times (M - \mathbf{x}^1_C). \end{aligned} \tag{42}$$

The question now is "How big should be the displacements $(\triangle \mathbf{x}, \triangle\theta)$?" Since we already computed the direction of the displacements the above question is reduced to the question of scaling "How big should be the scaling δ_t for $(\triangle \mathbf{x}, \triangle\theta) = \delta_t(\mathbf{v}, \omega)$?"

We should take δ_t so that swimmers are "slightly" out of contact.

For this we find the points O^1 and O^2 on the boundary of S^1 and S^2 that are between P_1 and P_2. For example take O^1 to be the point on the surface of S^1 (that is inside S^2), where the tangent line is parallel to the line through (P_1, P_2). Choose O^2 in a similar fasion. Compute the projection of O^1O^2 onto $\mathbf{n}_{(P_1,P_2)}$. Find the velocities $\mathbf{v}_{O^1}, \mathbf{v}_{O^2}$ of the points O^1 and O^2. Take

$$\delta_t := (1+\alpha)\frac{(O^1 - O^2)\cdot \mathbf{n}_{(P_1,P_2)}}{(\mathbf{v}_{O^1} - \mathbf{v}_{O^2})\cdot \mathbf{n}_{(P_1,P_2)}}.$$

Here $\alpha \geq 0$ is an analogue of a restitution coefficient (measure of bounce, i.e. elastic vs inelastic collision). It can, also, serve as a "reserve" to guaranty that after the procedure the ellipses do not overlap. We choose the coefficient $\alpha = .1$ to be small. This coerresponds to making collisions of the eclusion regions soft collisions.

4.4 Dynamics: Interaction of swimmers

Here we present two numerical experiments for the hydrodynamic interaction of swimmers at the intermediate distances (distances of order of the size of the swimmer): a swimmer next to a wall (see figure 5*a*) and two side-by-side swimmers (see figure 5*b*). In both cases attraction due to a hydrodynamic interaction was observed.

This behavior can be explained, heuristically, by the fact that each swimmer acts as a force dipole (5) – it pushes fluid forward ahead of itself (due to no-slip condition on Γ_H) and back behind itself (due to the thrust condition on Γ_ν). Since the fluid is incompressible, it is being forced towards the swimmer on its sides (creating lateral suction of sorts).

4.4.1 A swimmer next to a wall

In the case of a swimmer next to the wall (see figure 5*a*) the swimmer was positioned parallel to a wall a distance .1 away from the wall. The lengths of the semi-axes of the swimmer were $a = 0.048$ by $b = 0.024$. The propulsion force is given by (14) with the propulsion strength $f_p = 1$.

At the initial time the translational and rotational velocities of the swimmer was found to be

$$\mathbf{u}_C^1 = \begin{bmatrix} 0.0651970 \\ -0.0166068 \end{bmatrix}, \qquad \omega^1 = 0.06120. \tag{43}$$

The vertical component of the swimmer's velocity (due to the interaction with the wall) is roughly 1/4 of its forward component of the velocity (i.e. interaction with the wall is rather strong).

With time the swimmer approaches the wall, simultaneously rotating away from it. When rotated sufficiently far away from the wall, it starts swimming away.

Therefore, it was observed that a swimmer parallel to the wall is attracted to the wall, spending significant amount of time next and nearly parallel to it. But it will not remain next to the wall indefinitely. The whole time when near the wall, the swimmer rotates away from the wall and after a certain time swims away.

4.4.2 Two adjacent "mirror image" swimmers

Here we consider two swimmers with the length of the semi-axes $a = 0.048$ and $b = 0.024$, initially positioned parallel to the x-axes, with the centers on the same vertical line (see figure 5*b*):

$$\mathbf{x}_C^1 = \begin{bmatrix} .5 \\ .4 \end{bmatrix} \qquad \text{and} \qquad \mathbf{x}_C^2 = \begin{bmatrix} .5 \\ .6 \end{bmatrix}.$$

The swimmers 1 and 2 are mirror images of one another relative to the horizontal line $y = .5$ (hence the name "mirror image").

At the initial time the velocities of the swimmers were found to be

$$\mathbf{u}_C^{1,2} = \begin{bmatrix} 0.066246 \\ \pm 0.014640 \end{bmatrix}, \qquad \omega^{1,2} = \mp 0.0203. \tag{44}$$

With time the swimmers approach one another, simultaneously rotating away from one another. This dynamics of two side-by-side swimmers is reminiscent of the dynamics of two well-separated "external pushers" in a similar configuration [15]. There is a difference between the well-separated and moderately separated regimes, however. In the well separated regime the swimmers have enough time to rotate sufficiently away from one another for the translational correction (to swimming straight) due to the suction to be dominated by the vertical component of the velocity for a free swimmer (i.e., the velocity of the swimmer in the absence of the other swimmer). In the moderate regime the suction is too strong and the swimmers do not have enough time to rotate

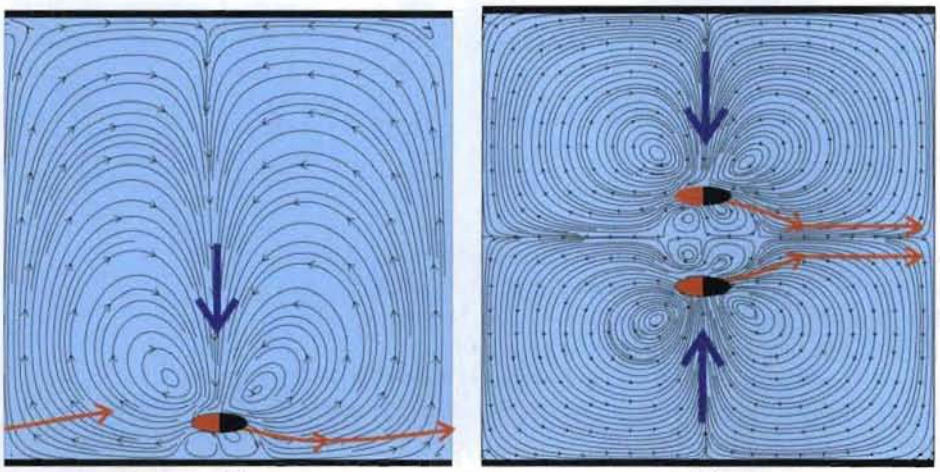

(*a*) (*b*)

Fig. 5 Figure *(a)* shows the fluid flow for a single microswimmer next to a wall. Figure *(b)* shows the fluid flow for two swimmers side by side. The bold blue arrows indicate the direction of the fluid that pushes the swimmer closer to the wall *(a)* and the two swimmers closer to one another *(b)*. The bold red lines with arrows indicate the trajectories that each of the swimmers will follow. Both *(a)* and *(b)* show the initial period of attraction (red line getting closer to the wall and two red lines getting closer to one another). The two swimmers in the mirror image configuration remain close to one another after this. The swimmer next to the wall rotates away from the wall to eventually get further and further away from it.

sufficiently outwards for the vertical component of the velocity due to a free swimmer to dominate the velocity due to suction.

One can also compare the velocities (44) and (45). While the translational velocities in both cases are almost the same, the rotational velocity in (45) is roughly three times larger than in (44). This may explain the difference in the dynamics between swimmer next to a wall and two "mirror image" swimmers.

In figure 5*(b)* one can clearly see the trajectories of the swimmers converge and experience a sharp turn after which they become parallel. In the case of swimmers positioned perfectly symmetrically (relative to a middle line between them) the swimmers would always remain in the symmetrical configuration ad remain and distance .0664 between their centers and at the angles $\mp.28$ (turned somewhat outwards) with the x-axes.

In case of the swimmers not in a perfectly symmetric configuration, the swimmers eventually separate and swim away from one another. This type of dynamics is illustrated by the "offset" configuration, presented below.

4.4.3 Two adjacent "offset" swimmers

Here we consider two swimmers parallel to the x-axes with the centers offset from the same vertical line (hence, the name "offset"):

$$\mathbf{x}_C^1 = \begin{bmatrix} .55 \\ .4 \end{bmatrix} \qquad \text{and} \qquad \mathbf{x}_C^2 = \begin{bmatrix} .45 \\ .6 \end{bmatrix}.$$

This initial configuration of swimmers can be thought of as a perturbation of the "mirror image" configuration.

At the initial time the velocities of the swimmers were found to be

$$\begin{aligned} \mathbf{u}_C^1 &= \begin{bmatrix} 0.062681 \\ 0.004727 \end{bmatrix}, \qquad \omega^1 = -0.1226, \\ \mathbf{u}_C^2 &= \begin{bmatrix} 0.0740155 \\ -0.006436 \end{bmatrix}, \qquad \omega^2 = -0.1113. \end{aligned} \tag{45}$$

In this configuration, initially, both of the swimmers rotate in the same direction (clockwise). The direction of the rotation is determined by which of the two swimmers is ahead of the other one. Here it is the first (bottom) swimmer. So, the second (top) swimmer rotates towards the first one (see the streamlines in Figure 6).

Eventually, swimmer two will cross the axes of the first swimmer behind it and will swim away, see figure 6. This demonstrates that there is no stable configuration of swimmers where they stay close to one another indefinitely.

4.5 Relation between the time and size scales in the physical and numerical experiments

In an attempt to relate the numerical unit of time to the physical unit of time we note the physical parameters of bacteria such as *Bacillus subtillis*. The length of the bacteria is around 5μm and (if they have enough oxygen) they swim with the speed of $\sim 100\mu$m/sec.

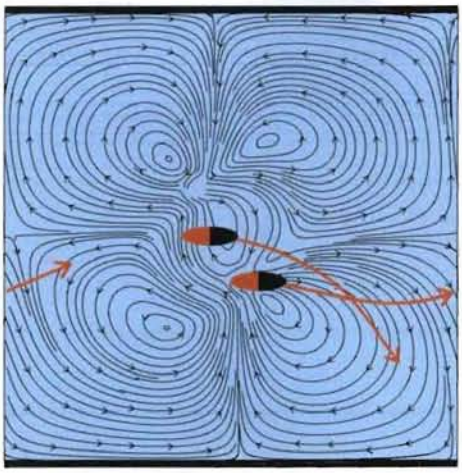

Fig. 6 Figure illustrates the fluid flow for two "offset" parallel microswimmer. Bold red lines show the trajectories each of the swimmers will follow.

The length of a swimmer in these numerical experiments next to a wall and next to another swimmer is $2a = 0.096$. In these experiments, (45) and (44), the typical forward component of the velocity of a swimmer is

$$.065 \approx \frac{2}{3} \frac{\text{swimmer body length}}{\text{computer unit of time}}. \tag{46}$$

Since the typical speed of bacteria (having enough oxygen) is 20 body lengths per second, the unit of computer time for $f_p = 1$ corresponds to

$$\left(\text{unit of computer time for} f_p = 1\right) = \frac{2/3}{20} \text{ sec.} = 1/30 \text{ sec.} \tag{47}$$

Now we compute the physical analog of the shear rate for the computational experiment with $f_p = 1$. The total size of the domain is $1/.096 \approx 10$ lengths of a swimmer, which corresponds to 50μm. The speed of each (top and bottom) plates is $\frac{50\mu\text{m}}{1/30\text{sec}} = 1.5\frac{\text{mm}}{\text{sec}}$. The shear rate is 30 sec^{-1}.

4.6 Effective viscosity

For a homogeneous fluid, the instantaneous apparent viscosity defined by (24) and the effective viscosity defined by (25) are the same thing. For an inhomogeneous fluid (e.g., suspensions) (24) will take different values depending on the distribution of inclusions. Figure 7 illustrates a sample measurements of the instantaneous apparent viscosity for a suspension of swimmers as a function of time.

Since in practice the instantaneous apparent viscosity is measured on a finite interval of time it is important to produce an error estimate for the effective viscosity, which is not trivial. Intuitively, it seams that the more measurements one makes (i.e., more time steps) the more accurate is the estimate of the effective viscosity. This is true only in part. The same number of measurements (time steps) can be done with small or

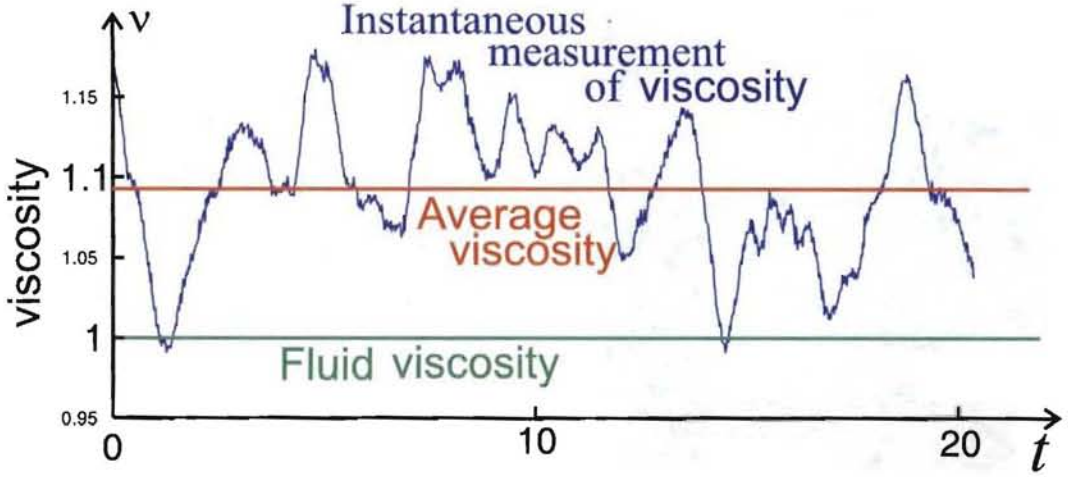

Fig. 7 The green horizontal line indicates the viscosity of the ambient fluid ($\mu = 1$). The blue (oscillating) line shows the instantaneous measurements of viscosity for the suspension of swimmers, as defined by (24). The red horizontal line indicates the time average of the instantaneous measurements of viscosity for the suspension of swimmers. The measurements are performed for the suspension of 25 swimmers at 9% volume fraction in a 1 by 1 square with 1-periodic boundary conditions in x-direction. The propulsion of each swimmer is defined by (14) with the total propulsion strength $f_p = 1$ as defined by (15).

large time step $\triangle t$. Small $\triangle t$ is important for correctly capturing the dynamics of the suspension. Long total time range of the measurements is important for the accuracy of the overall estimate of the effective viscosity as the mean of the instantaneous apparent viscosity. In the extremes, million measurements with time step 10^{-12} or hundred measurements with time step 10 may be equally poor at predicting the effective viscosity. In the first case one would get a a very accurate dynamics of the suspension, but would miss the range of values. In the second case one would get a rather broad range of values for completely inaccurate dynamics of the suspension. Since the interaction of swimmers is assumed to play a key role in the effective viscosity of the suspension the last choice is not satisfactory as well.

In our analysis we begin by identifying an acceptable time step, which may be a subjective quantity. As a criteria we set the condition that time step is much smaller than the time required for significantly changing the instantaneous apparent viscosity of the suspension. For the propulsion-shear ratio $f_p/v = 1$ the appropriate time step was chosen to be $\triangle t_1 = .02$. Based on this choice and the scaling argument 1 for the propulsion-shear ratio $f_p/v = \lambda > 0$ the appropriate time step was chosen to be $\triangle t_\lambda = \triangle t_1/\lambda$.

A sample mean of N independent identically distributed random variables approaches normal distribution with the standard deviation $s/\sqrt{N}$, where s is the standard deviation of the underlying distribution. In our analysis all measurements of the instantaneous apparent viscosity do not represent independent sample. For example the correlation between the values of instantaneous apparent viscosity on the adjacent time steps is more than .8 for propulsion-shear ratio $f_p/v = 1$. We find the smallest lag n_{lag} when the autocorrelation equals to 0. For the case of propulsion-shear ration $f_p/v = 1$, figure 9, the zero-autocorrelation lag is $n_{\text{lag}} = 58$. This number indicates

that the measurements on time-step n_{lag} apart are essentially uncorrelated and may be viewed as independent sample.

The total number of time steps divided by n_{lag} is the sample size N. The error in estimating the effective viscosity is then assumed to have a normal distribution with the standard deviation

$$\text{standard deviation} = \frac{\text{standard deviation of the measurements}}{\sqrt{N_{\text{total}}/n_{\text{lag}}}}. \tag{48}$$

The standard deviation of the error computed according to (48) is sketched on Figure 8.

4.6.1 Effective viscosity as a function of propulsion-shear ratio

In this section we are looking for the dependence of the effective viscosity on the propulsion-shear ratio f_p/v. To compute the effective viscosity we make the following numerical experiments. First, we fix the dimensions of the container to be 1 by 1 square with appropriate boundary conditions. The shear velocity is taken to be 1. We fix the size and number (hence volume fraction) of swimmers and vary only the propulsion strength f_p of the swimmers. For each value of the propulsion strength we simulate the dynamics of the swimmers, computing the pressure and the velocity of the fluid and swimmers. Knowing the velocity and pressure solutions allows us to compute the viscous forces acting on the top and bottom plates, and hence the instantaneous value of the instantaneous apparent viscosity as defined by (24).

The effective viscosity as a function of the propulsion strength is shown on Figure 8. One can notice that the standard deviation of the estimates for the effective viscosity on Figure 8 generally is much larger for larger values of the propulsion-shear ratio f_p/v. This is due to the fact that the standard deviation of the instantaneous apparent viscosity is proportional to the propulsion strength of the swimmers. Therefore, according to the error estimate (48) to compute the effective viscosity for $f_p/v = 10$ with the same accuracy as for $f_p/v = 1$ it requires not 10 but 10^2 more time steps.

The red line on Figure 8 is given by

$$\hat{\mu}(f_t) = \alpha f_p + \beta, \qquad \alpha = -0.0351 \qquad \beta = 1.1407, \tag{49}$$

and represents the waited least square fit to the data. It minimizes

$$\min_{\alpha,\beta\in\mathbb{R}} \sum_i \frac{(\hat{\mu}_i - \alpha f_p^i - \beta)^2}{s_i^2}, \tag{50}$$

where f_p^i are the values for which the estimate of the effective viscosity $\hat{\mu}_i$ is computed.

The estimates of the effective viscosity for the propulsion-shear ratio $f_p/v = -1, 0, 1, 2, 3, 4, 5$ is consistent with the linear decrease of the effective viscosity. For the values of the propulsion-shear ratio $f_p/v > 5$ the linear trend seams to change. We explain this change by the finite size of the fluid domain. To illustrate that the trend changes around the value of the propulsion-shear ratio $f_p/v \sim 6$ we show the dynamics of a single swimmer for the propulsion-shear ratios of $f_p/v = 1$ and 6, see Figure **??**. Since the shear background flow rotates a swimmer and a swimmer by itself swims on a straight line, a single swimmer in a shear background flow will have an ellipse as the trajectory. The larger is the the propulsion-shear ratio the larger is the ellipse-like trajectory of the swimmer. For the propulsion-shear ratio of $f_p/v \sim 6$ the ellipse-like trajectory of the swimmer cannot fit into the fluid domain any more.

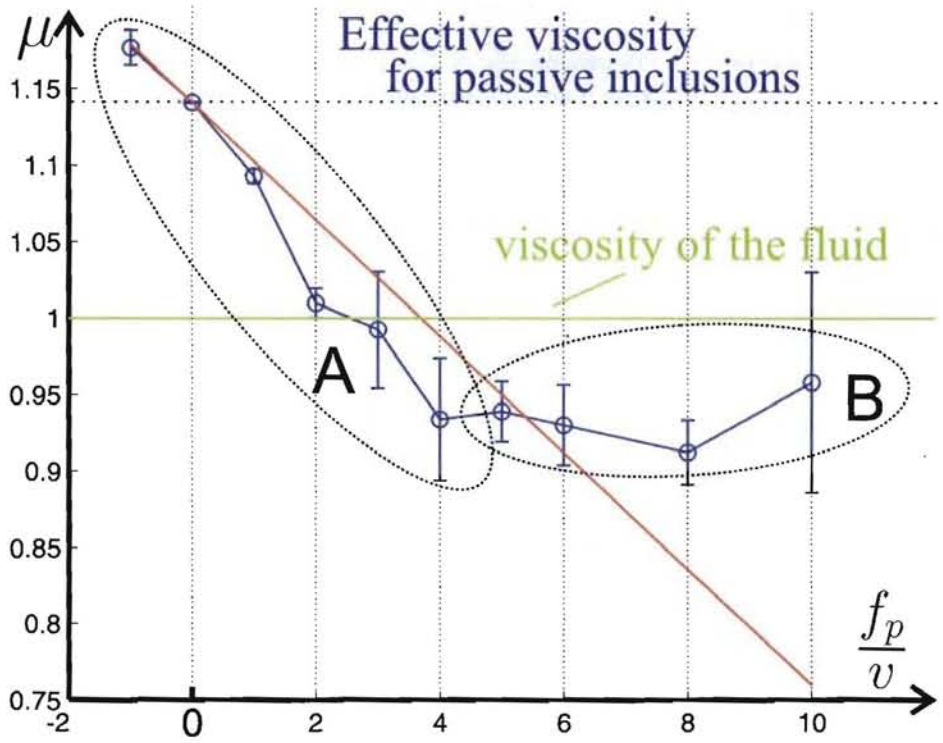

Fig. 8 Circles indicate the numerically obtained values of the effective viscosity for a given propulsion-shear ratio f_p/v. The points are combined into two groups: **A** and **B**. Points in group **A** exhibit linear trend. Points in group **B** exhibit finite domain effects. The solid horizontal line shows the viscosity of the ambient fluid ($\mu = 1$). The dashed horizontal line shows the effective viscosity of a suspension of passive inclusions ($f_p = 0$). The decline straight line shows the weighted linear interpolation to the data.

4.6.2 Distribution of swimmers in the domain

The distribution of swimmers in the domain and their orientations plays a crucial role in determining the instantaneous apparent viscosity.

In physical experiments [17,31,4] it was observed that swimmers tend to aggregate near the walls. In our numerical experiments we observed this aggregation through computing the time averaged volume density of swimmers as a function of distance from the bottom wall (see figure 10). That is, given a number d we drew a horizontal line distance d from the bottom wall and computed the portion of the line covered by swimmers. This number is the volume fraction of swimmers at depth d and it fluctuates as swimmers move within the domain. To get rid of the fluctuations we take a time average of the volume fractions for the same depth d. Due to the top-bottom symmetry of the PDE and the random initial conditions, the graph of the distribution is symmetric under transformation $d \leftrightarrow (1 - d)$, as expected.

For instance in [16] it was demonstrated that in the absence of pairwise interactions, shear flow leads to a distribution of swimmers by the angles that decreases the viscosity.

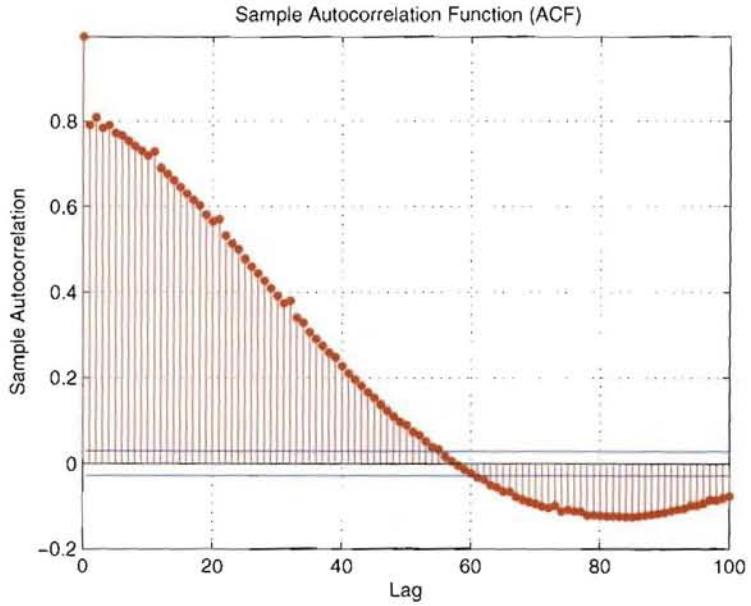

Fig. 9 Autocorrelation function for $f_p = 1$ and time step $\triangle t = .02$.

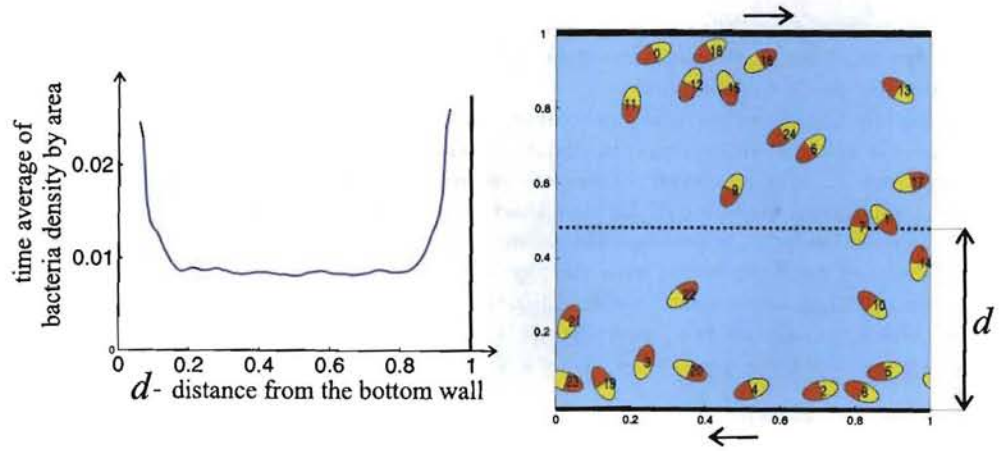

Fig. 10 The figure on the right shows a sample distribution of swimmers in the domain. The figure on the left shows that time-averaged volume fraction of swimmers as a function of the depth (distance from the bottom wall). Here we took 25 swimmers with the propulsion strength $f_p = 1$ with the overall volume fraction of swimmers .09. One can observe the increase of the density near the top and bottom walls.

In the presence of the pairwise interactions and swimmer-wall interactions the dynamics of the swimmers is much more complex.

5 Summary

In this work we formulated a well-posed PDE model for the suspension of swimmers, which includes the propulsion strength f_p of the swimmers as a parameter.

Using the symmetries of the model we demonstrated that in the dilute regime (each swimmer interacts only with the background flow) the effective shear viscosity of a suspension of swimmers does not depend on the propulsion strength. This argument is not specific to our choice of a swimmer and can be applied to a large class of swimmers without significant changes. In particular it can be applied to the swimmers in [18,28, 16].

Using the invariance of the PDE model under scaling we observed the dependence of the effective shear viscosity on the ratio of the propulsion strength to the shear rate of the background flow, called propulsion-shear ratio.

Our numerical simulations performed at the moderate concentrations ($\sim$ 10% by volume) indicate that the effective shear viscosity decays linearly as a function of the propulsion-shear ratio of f_p/v. This continues to hold for negative values of the propulsion strength, which corresponds to swimmers swimming in the opposite direction, i.e. pullers instead of pushers. Performing the experiment in a finite container places an upper bound on the propulsion-shear ratio for which the effective shear viscosity changes linearly. The value of propulsion-shear ratio is such that a single swimmer following an ellipse-like trajectory (due to rotation by the background flow) will "touch" both upper and lower boundaries of the domain. The numerical experiments in the moderate concentration indicate that the decrease of the effective viscosity observed in the physical experiments can be explained entirely from a point of view of hydrodynamics. This is an important observation, since biological system are very complex and include a variety of processes (chemotaxis, oxygen taxis, etc.) that could be hard to isolate in physical experiments. On the other hand our mathematical model does not contain all the excess phenomena and focuses on on the hydrodynamics.

Comparing the results for the effective shear viscosity in the dilute and moderate concentration regimes shows changes (increase or decrease) in effective shear viscosity are not just due to self-propulsion but crucially depend on the swimmer-swimmer interactions. For this reason and as an additional validation of the model and the numerical approach we performed a number of simulation for two nearby swimmers and for a swimmer next to a wall. The observed results matched with the physically observed behavior for bacteria. In all cases swimmers attract one another due to lateral suction of fluid, resulting from self propulsion. But neither two swimmers nor a swimmer next to a wall have a steady state in terms of relative positions.

6 Acknowledegements

The work of the first and the second authors was supported in part by the DOE Office of Science Advanced Scientific Computing Research (ASCR) Program in Applied Mathematics Research.

A Variational formulation for the instantaneous problem (1-6)

There are a number of questions that are easier answered working with the variational formulation of the problem instead of the PDE. Here we refer to the instantaneous PDE problem

(1-6). The questions that plan to answer are well-posedness of the problem (existence and uniqueness of the solution) and construction of the numerical scheme for approximating the solution to (1-6).

For simplicity of presentation, we will derive the variational formulation for a single swimmer. Obtaining the variational formulation for multiple swimmers after that will be straightforward.

First, we specify the admissible class $\mathcal{A}_{\mathbf{g}}$ of solutions $\mathbf{u}$ and then the space $\mathcal{A}_0$ of variations $\mathbf{v}$. The admissible class of velocity fields $\mathbf{u}$ is defined as

$$\mathcal{A}_{\mathbf{g}} := \left\{ \mathbf{u} \in H^1(\Omega_F) \;\middle|\; \begin{array}{ll} \mathbf{u}(\mathbf{x}) = \mathbf{g}(\mathbf{x}) & \text{for } \mathbf{x} \in \partial\Omega, \\ \mathbf{u}(\mathbf{x}) = \mathbf{u}_C + \omega_{\mathbf{u}} \times (\mathbf{x} - \mathbf{x}_C) & \text{for } \mathbf{x} \in \Gamma_H, \\ \mathbf{u}(\mathbf{x}) = \mathbf{u}_C + \omega_{\mathbf{u}} \times (\mathbf{x} - \mathbf{x}_C) + \tau\tilde{u} & \text{for } \mathbf{x} \in \Gamma_P \end{array} \right\}. \tag{51}$$

Here τ is a unit tangent to the surface and $\tilde{u}$ is an unknown scalar function.

The linear space $\mathcal{A}_0$ of variations for the admissible class $\mathcal{A}$ is

$$\mathcal{A}_0 := \left\{ \mathbf{v} \in H^1(\Omega_F) \;\middle|\; \begin{array}{ll} \mathbf{v}(\mathbf{x}) = 0 & \text{for } \mathbf{x} \in \partial\Omega, \\ \mathbf{v}(\mathbf{x}) = \mathbf{v}_C + \omega_{\mathbf{v}} \times (\mathbf{x} - \mathbf{x}_C) & \text{for } \mathbf{x} \in \Gamma_H, \\ \mathbf{v}(\mathbf{x}) = \mathbf{v}_C + \omega_{\mathbf{v}} \times (\mathbf{x} - \mathbf{x}_C) + \tau\tilde{v} & \text{for } \mathbf{x} \in \Gamma_P \end{array} \right\}. \tag{52}$$

Rewrite the Stokes equation (1) by adding to its LHS

$$\mu \operatorname{div}(\nabla \mathbf{u})^T = \mu \nabla(\operatorname{div} \mathbf{u}) = 0.$$

We obtain

$$2\mu \operatorname{div}\left(D(\mathbf{u})\right) = \nabla p. \tag{53}$$

This is done to obtain symmetrized gradient $D(\mathbf{u})$ (and later a stress tensor $\sigma(\mathbf{u}, p)$) in place of $\nabla \mathbf{u}$. Multiply (53) by $\mathbf{v} \in \mathcal{A}_0$ and integrate over Ω_F

$$\int_{\Omega_F} \left(2\mu \operatorname{div}\left(D(\mathbf{u})\right) - \nabla p\right) \cdot \mathbf{v} \, d\mathbf{x} = 0. \tag{54}$$

Integrate (54) by parts (here $\mathbf{n}$ is a unit outward normal to the boundary)

$$\begin{aligned} -2\mu \int_{\Omega_F} D(\mathbf{u}) : \nabla \mathbf{v} \, d\mathbf{x} + 2\mu \int_{\partial\Omega_F} \mathbf{n} D(\mathbf{u}) \mathbf{v} \, d\mathbf{x} + \\ + \int_{\Omega_F} p \operatorname{div}(\mathbf{v}) \, d\mathbf{x} - \int_{\partial\Omega_F} p \mathbf{v} \mathbf{n} \, d\mathbf{x} = 0. \end{aligned} \tag{55}$$

Combining the second and forth terms in (55), using the definition of

$$\sigma(\mathbf{u}, p) := 2\mu D(\mathbf{u}) - pI, \tag{56}$$

and rearranging the remaining terms

$$2\mu \int_{\Omega_F} D(\mathbf{u}) : \nabla \mathbf{v} \, d\mathbf{x} - \int_{\Omega_F} p \operatorname{div}(\mathbf{v}) \, d\mathbf{x} = \int_{\partial\Omega_F} \mathbf{n} \sigma(\mathbf{u}, p) \mathbf{v} \, d\mathbf{x}. \tag{57}$$

Consider the last integral $\int_{\partial\Omega_F} \mathbf{n}\sigma(\mathbf{u}, p)\mathbf{v} \, d\mathbf{x}$ and note that

$$\partial\Omega_F = \partial\Omega \cup \partial B, \qquad \text{where } \partial B = \Gamma_H \cup \Gamma_P.$$

Due to the boundary conditions (3-6)on the solution $\mathbf{u}$ and the boundary conditions (52) on the test function $\mathbf{v}$ we have

$$\int_{\partial\Omega} \mathbf{n} \sigma(\mathbf{u}, p) \mathbf{v} \, d\mathbf{x} = 0. \tag{58}$$

The integral over the surface of bacteria can be written as

$$\begin{aligned}\int_{\partial B} \mathbf{n}\sigma(\mathbf{u},p)\mathbf{v}\ d\mathbf{x} &= \int_{\partial B} \mathbf{n}\sigma(\mathbf{u},p)(\mathbf{v}_C + \omega_{\mathbf{v}} \times (\mathbf{x}-\mathbf{x}_C) + \tau\tilde{v})\ d\mathbf{x} = \\ &= \mathbf{v}_C \cdot \int_{\partial B} \mathbf{n}\sigma(\mathbf{u},p)\ d\mathbf{x} + \omega_{\mathbf{v}} \int_{\partial B} (\mathbf{x}-\mathbf{x}_C) \times \mathbf{n}\sigma(\mathbf{u},p)\ d\mathbf{x} + \\ &+ \int_{\Gamma_P} \mathbf{n}\sigma(\mathbf{u},p)\tau\tilde{v}\ d\mathbf{x} = \\ &= \mathbf{v}_C \cdot (\mathbf{F}_H + \mathbf{F}_P) + \omega_{\mathbf{v}}(\mathbf{T}_H + \mathbf{T}_P) + \int_{\Gamma_P} \mathbf{n}\sigma(\mathbf{u},p)\tau\tilde{v}\ d\mathbf{x}.\end{aligned} \tag{59}$$

Since

$$(\mathbf{F}_H + \mathbf{F}_P) = 0, \qquad \mathbf{v}_C \cdot (\mathbf{F}_H + \mathbf{F}_P) = 0.$$

Since

$$(\mathbf{T}_H + \mathbf{T}_P) = 0, \qquad \omega_{\mathbf{v}}(\mathbf{T}_H + \mathbf{T}_P) = 0.$$

Since

$$\mathbf{n}\sigma(\mathbf{u},p)\tau = \frac{-f_p}{|\Gamma_P|}(\mathbf{d}\cdot\tau),$$

the integral takes form

$$\begin{aligned}\int_{\Gamma_\mu} \mathbf{n}\sigma(\mathbf{u},p)\tau\ \tilde{v}\ d\mathbf{x} &= -\int_{\Gamma_P} \frac{f_p}{|\Gamma_P|}(\mathbf{d}\cdot\tau)\tilde{v}\ d\mathbf{x} = \\ &= -\frac{f_p}{|\Gamma_P|}\mathbf{d}\cdot\left[\int_{\Gamma_P} \tau\tilde{v}\ d\mathbf{x} + \int_{\Gamma_\mu} \mathbf{v}_C\ d\mathbf{x} + \int_{\Gamma_P} \omega^{\mathbf{v}} \times (\mathbf{x}-\mathbf{x}_C)\ d\mathbf{x}\right] + \\ &+ \frac{f_p}{|\Gamma_H|}\mathbf{d}\cdot\left[\int_{\Gamma_H} \mathbf{v}_C\ d\mathbf{x} + \int_{\Gamma_H} \omega^{\mathbf{v}} \times (\mathbf{x}-\mathbf{x}_C)\ d\mathbf{x}\right] = \\ &= \frac{f_p}{|\Gamma_P|}\mathbf{d}\cdot\left[-\int_{\Gamma_P} \mathbf{v}\ d\mathbf{x} + \int_{\Gamma_H} \mathbf{v}\ d\mathbf{x}\right],\end{aligned}$$

which is a known linear functional of $\mathbf{v}$.

Introduce the notations

$$a(\mathbf{u},\mathbf{v}) := \mu\int_{\Omega_F} D(\mathbf{u}) : \nabla\mathbf{v}\ d\mathbf{x} = \mu\int_{\Omega_F} D(\mathbf{u}) : D(\mathbf{v})\ d\mathbf{x}, \tag{60}$$

$$(p, \mathrm{div}(\mathbf{v})) := \int_{\Omega_F} p\,\mathrm{div}(\mathbf{v})\ d\mathbf{x}, \tag{61}$$

$$L(\mathbf{v}) := \frac{f_p}{|\Gamma_P|}\mathbf{d}\cdot\left[-\int_{\Gamma_P} \mathbf{v}\ d\mathbf{x} + \int_{\Gamma_H} \mathbf{v}\ d\mathbf{x}\right]. \tag{62}$$

Here τ is a unit tangent to the boundary, pointing forward relative to $\mathbf{d}$ on Γ_H and backward relative to $\mathbf{d}$ on Γ_P.

In the notations (60-62) equation (57) takes form

$$2a(\mathbf{u},\mathbf{v}) - (p, \mathrm{div}\,\mathbf{v}) = L(\mathbf{v}), \qquad \forall\mathbf{v} \in \mathcal{A}_0. \tag{63}$$

Take the incompressibility equation in (1), multiply by $q \in L_0^2(\Omega_F)$ and integrate over the fluid domain Ω_F to get

$$\int_{\Omega_F} \mathrm{div}(\mathbf{u})q\ d\mathbf{x} = (q, \mathrm{div}\,\mathbf{u}) = 0, \qquad \forall q \in L_0^2(\Omega_F). \tag{64}$$

Combining equations (63-64) we have a complete variational formulation:
Find a pair $(\mathbf{u},p)$, $\mathbf{u} \in \mathcal{A}_\mathbf{g}$ and $p \in L_0^2(\Omega_F)$, such that

$$\begin{cases} 2a(\mathbf{u},\mathbf{v}) - (p, \mathrm{div}\,\mathbf{v}) = L(\mathbf{v}), & \forall\mathbf{v} \in \mathcal{A}_0, \\ (q, \mathrm{div}\,\mathbf{u}) = 0, & \forall q \in L_0^2(\Omega_F). \end{cases} \tag{65}$$

The minimization problem, corresponding to the variational problem (65) is:

$$\min_{\mathbf{u}\in\mathcal{A}_{\mathbf{g}}^{\mathrm{div}=0}} E[\mathbf{u}], \qquad \text{where } E[\mathbf{u}] := a(\mathbf{u},\mathbf{u}) - L(\mathbf{u}) \tag{66}$$

and $\mathcal{A}_{\mathbf{g}}^{\mathrm{div}=0}$ consists of divergence free functions from $\mathcal{A}_{\mathbf{g}}$.

B Well posedness of the instantaneous PDE problem (1-6)

The minimization problem corresponding to the variational formulation (65) is to minimize

$$E[\mathbf{u}] := a(\mathbf{u},\mathbf{u}) - L(\mathbf{u}) \tag{67}$$

over all

$$\mathbf{u} \in \mathcal{A}_{\mathbf{g}} \cup H_{\mathrm{div}=0}. \tag{68}$$

The existence and uniqueness of minimizers of (67) is proved in a standard way provided that the coercivity of the bilinear form $a(\cdot,\cdot)$ can be shown. The coercivity proof, using Korn's inequality, is essentially contained in [11] as we now explain.

Theorem 1 *The bilinear form $a(\cdot,\cdot)$ is coercive on V with respect to the norm $||\cdot||_1$ induced from $H^1(\Omega_F)$. In particular, $a(\cdot,\cdot)$ defines an equivalent inner product on V.*

Proof Coercivity of $a(\cdot,\cdot)$ relies in an essential way on Korn's inequality:

$$a(\mathbf{u},\mathbf{u}) + ||\mathbf{u}||^2 > c\,||\mathbf{u}||_1^2, \tag{69}$$

for some $c > 0$ (here $||\cdot||$ denotes the L_2 norm). The proof of (69) found in [11] applies to the case for any subspace $U \subset H^1(\Omega_F))$ consisting of functions with a zero trace on a part of the boundary with nonzero two-dimensional measure. This applies to V as its elements vanish on $\partial\Omega$ – the no-slip boundary conditions on the outer boundary of Ω_F. In particular, $a(\cdot,\cdot)$ is nondegenerate, since the nontrivial kernel of $D(\mathbf{u})$, consisting of the rigid motions $\mathbf{u}(\mathbf{x}) = \mathbf{u}_0 + \omega_0 \times \mathbf{x}$, is excluded from V due these boundary conditions. The result (69) is nontrivial, since the left-hand side contains only symmetric combinations of the derivatives of $\mathbf{u}$.

The coercivity proof is completed by showing the existence of the following bound:

$$a(\mathbf{u},\mathbf{u}) > d||\mathbf{u}||^2, \tag{70}$$

for some $d > 0$. This replaces Poincare's inequality in the case of the symmetrized gradient. It can be proved for V as is done in [11], using the compactness of the embedding $V \hookrightarrow L_2(\Omega_F)$. This embedding is induced from the usual compact embedding $H^1(\Omega_F) \hookrightarrow L_2(\Omega_F)$, since V, being a closed subspace of $H^1(\Omega_F)$ is also weakly closed (see, e.g., [20]).

With the coercivity of $a(\cdot,\cdot)$ proved, the existence of minimizers for (67) can be proved by standard techniques. Since each minimizer satisfies (55), the difference of any two of them is $a(\cdot,\cdot)$-orthogonal to a dense subset of V, hence is zero, which proves uniqueness.

Finally, the unique field $\mathbf{u}$ that solves (67) is a weak solution of the Stokes equation on a regular bounded domain. Therefore, once again by the standard theory (e.g., [13]), there exists a unique pressure field $p \in L_2(\Omega_F)$, which together with $\mathbf{u}$ satisfies the a priori L_2 estimates [13]. Since the boundary of Ω_F and the is smooth, these estimates imply that $(\mathbf{u}, p)$ are smooth too. By reversing the steps leading to the weak formulation (55), we now see that $(\mathbf{u}, p)$ form a strong solution of the full system.

References

1. G. K. Batchelor. The stress system in a suspension of force-free particles. *Journal of Fluid Mechanics*, 41:545–570, 1970.
2. G. K. Batchelor and J. T. Green. The determination of the bulk stress in a suspension of spherical particles to order c^2. *Journal of Fluid Mechanics*, 56:401–427, 1972.
3. L. Beirão da Veiga, V. Gyrya, , K. Lipnikov, and G. Manzini. Mimetic finite difference method for the stokes problem on polygonal meshes. *submitted to J. Comp. Phys.*, 2009.
4. Allison P. Berke, Linda Turner, Howard C. Berg, and Eric Lauga. Hydrodynamic attraction of swimming microorganisms by surfaces. *Phys. Rev. Lett.*, 101:038102, 2008.
5. L. Berlyand, Y. Gorb, and A. Novikov. Fictitious fluid approach and anomalous blow-up of the dissipation rate in a 2D model of concentrated suspensions. *Arch. Ration. Mech. Anal.*, 193(3):585–622, 2009.
6. L. Berlyand and A. Panchenko. Strong and weak blow up of the viscous dissipation rates for concentrated suspensions. *Journal of Fluid Mechanics*, 578:1–34, 2007.
7. Leonid Berlyand, Liliana Borcea, and Alexander Panchenko. Network approximation for effective viscosity of concentrated suspensions with complex geometry. *SIAM J. Math. Anal.*, 36(5):1580–1628 (electronic), 2005.
8. F. Brezzi, K. Lipnikov, M Shashkov, and V. Simoncini. A new discretization methodology for diffusion problems on generalized polyhedral meshes. *Comput. Methods Appl. Mech. Engrg.*, 196:3682–3692, 2007.
9. M. E. Cates, S. M. Fielding, D. Marenduzzo, E. Orlandini, and J. M. Yeomans. Shearing active gels close to the isotropic-nematic transition. *Phys. Rev. Lett.*, 2008:068102:1–4, 2008.
10. Rémi Dreyfus, Jean Baudry, Marcus L. Roper, Marc Fermigier, Howard A. Stone, and Jérôme Bibette. Microscopic artificial swimmers. *Nature*, 437(7060):862–865, 2007.
11. G. Duvaut and J. L. Lions. *Inequalities in Mechanics and Physics*. Springer, 1976.
12. A. Einstein. A new determination of the molecular dimensions. *Annalen der Physik*, 19 (2):289–306, 1906.
13. G. P. Galdi. *An Introduction to the Mathematical Theory of the Navier-Stokes Equations*. Springer, 1994.
14. Ramin Golestanian and Armand Ajdari. Mechanical response of a small swimmer driven by conformational transitions. *Physical Review Letters*, 100:038101, 2008.
15. V. Gyrya, L. Berlyand, I. Aranson, and D. Karpeev. A model of hydrodynamic interaction between swimming bacteria. *Bulletin of Math. Biology*, 2009.
16. B.M. Haines, I.S. Aranson, L Berlyand, and D.A. Karpeev. Effective viscosity of dilute bacterial suspensions: A two-dimensional model. *preprint*, 2008.
17. J.P. Hernandez-Ortiz, Ch.G. Stoltz, and M.D. Graham. Transport and collective dynamics in suspensions of confined swimming particles. *Physical Review Letters*, 95:204501:1–4, 2005.
18. T. Ishikawa and T. J. Pedley. The rheology of a semi-dilute suspension of swimming model micro-organisms. *J. Fluid Mech.*, 588:399–435, 2007.
19. G. B. Jeffery. The motion of ellipsoidal particles immersed in a viscous fluid. *R. Soc. London Ser. A*, 102:161–79, 1922.
20. P. Lax. *Functional Analysis*. Wiley-Interscience, 2003.
21. L. G. Leal and E. J. Hinch. The effect of weak brownian rotations on particles in shear flow. *Journal of Fluid Mechanics*, 46(4):685–703, 1971.
22. L. G. Leal and E. J. Hinch. The effect of brownian motion on the rheological properties of a suspension of non-spherical particles. *Journal of Fluid Mechanics*, 52(4):683–712, 1972.
23. T. Levy and E. Sanchez-Palencia. Suspension of solid particles in a newtonian fluid. *Journal of Fluid Mechanics*, 56:401–427, 1983.
24. A. Najafi and R. Golestanian. Simple swimmer and low reynolds number: Three linked spheres. *Phys. Rev. E*, 69:062901, 2004.
25. S. Nasseri and N. Phan-Thien. Hydrodynamic interaction between two nearby swimming micromachines. *Computational Mechanics*, 20:551–559, 1997.
26. K. C. Nunan and J. B. Keller. Effective viscosity of periodic suspensions. *J. Fluid Mech.*, 142:269–287, 1984.
27. E.M. Purcell. Life at low Reynolds number. *American Journal of Physics*, 309(45):3–11, 1977.
28. S. Saintillan and M. Shelley. Orientational order and instabilities in suspensions of self-locomoting rods. *submitted*, 2007.

29. A. Sokolov and I. S. Aranson. Reduction of viscosity in suspension of swimming bacteria. *submitted to Physical Review Letters*, 2009.
30. A. Sokolov, I.S. Aranson, J.O. Kessler, and R.E. Goldstein. Concentration dependence of the collective dynamics of swimming bacteria. *Physical Review Letters*, 98:158102, 2007.
31. P. T. Underhill, J. P. Hernandez-Ortiz, and M. D. Graham. Diffusion and spatial correlations in suspensions of swimming particles. *Phys. Rev. Lett.*, 100:248101–1–4, 2008.
32. Xiao-Lun Wu and Albert Libchaber. Particle diffusion in a quasi-two-dimensional bacterial bath. *Physical Review Letters*, 84(13):3017–3020, March 2000.